Centimeter to decimeter hollow concretions and voids in Gale Crater sediments, Mars

Centimeter to Decimeter Hollow Concretions and Voids In Gale Crater Sediments, Mars

Roger C. Wiens[1], David M. Rubin[2], Walter Goetz[3], Alberto G. Fairén[4], Susanne P. Schwenzer[5], Jeffrey R. Johnson[6], Ralph Milliken[7], Ben Clark[8], Nicolas Mangold[9], Kathryn M. Stack[10], Dorothy Oehler[11], Scott Rowland[12], Marjorie Chan[13], David Vaniman[14], Sylvestre Maurice[15], Olivier Gasnault[15], William Rapin[15], Susanne Schroeder[16], Sam Clegg[1], Olivier Forni[15], Diana Blaney[10], Agnes Cousin[15], Valerie Payré[17], Cecile Fabre[17], Marion Nachon[18], Stephane Le Mouelic[9], Violaine Sautter[19], Stephen Johnstone[1], Fred Calef[10], Ashwin R. Vasavada[10], John P. Grotzinger[20]

[1]Los Alamos National Laboratory, Los Alamos, NM, USA

[2]Department of Earth & Planetary Sciences, University of California-Santa Cruz, Santa Cruz, CA, USA

[3]Max Planck Institute for Solar System Research, Göttingen, Germany

[4]Department of Planetology and Habitability, Centro de Astrobiología (CSIC-INTA), Madrid, Spain; and Department of Astronomy, Cornell University, Ithaca, NY, USA

[5]Dept. of Environment, Earth and Ecosystems, The Open University, Milton Keynes, UK

[6]Johns Hopkins University Applied Physics Laboratory, Laurel, MD, USA

[7]Brown University, Providence, RI, USA

[8]Space Science Institute, Boulder, CO, USA

[9]Université de Nantes, Laboratoire de Planétologie et Géodynamique, Nantes, France

[10]Jet Propulsion Laboratory, California Institute of Technology, Pasadena, CA, USA

[11]LZ Technology, NASA Johnson Space Center, Houston, TX, USA

[12]University of Hawaii, Manoa, HI, USA

[13]University of Utah, Salt Lake City, UT, USA

[14]Planetary Science Institute, Tucson, AZ, USA

[15]Université de Toulouse, UPS-OMP, Toulouse, France, and Institut de Recherche en Astrophysique et Planétologie, CNRS, UMR 5277, Toulouse, France

[16]German Aerospace Center (DLR), Institut für Optische Sensorsysteme, Berlin-Adlershof, Germany

[17]GeoRessources, Université de Lorraine, Nancy, France

[18]University of California-Davis, Davis, CA, USA

[19]IMPMC, Museum d'Histoire Naturelle de Paris, Paris, France

[20]California Institute of Technology, Pasadena, CA, USA

Submitted to *Icarus* July 9, 2016

Submitted in revised form January 28, 2017

Corresponding author:

Roger C. Wiens
rwiens@lanl.gov
MS C331, Los Alamos National Laboratory, Los Alamos, NM 87544, USA
Office phone: 505-667-3101

Keywords: Concretions, voids, spherules, nodules, Gale crater, Mars, Mars Science Laboratory

Highlights (also submitted as a separate file)**:**

- Hollow spheroids to > 20 cm, interpreted as concretions, are found in Gale crater
- The hollow concretions are found together with spheroidal voids
- Large hollow, rounded concretions have not been found at other Mars landing sites
- Localized redox reactions can produce hollow concretions in terrestrial sediments
- The high Fe content of Mars sandstones may facilitate production of concretions

Abstract

Voids and hollow spheroids between ~1 and 23 cm in diameter occur at several locations along the traverse of the Curiosity rover in Gale crater, Mars. These hollow spherical features are significantly different from anything observed in previous landed missions. The voids appear in dark-toned, rough-textured outcrops, most notably at Point Lake (sols 302-305) and Twin Cairns Island (sol 343). Point Lake displays both voids and cemented spheroids in close proximity; other locations show one or the other form. The spheroids have 1-4 mm thick walls and appear relatively dark-toned in all cases, some with a reddish hue. Only one hollow spheroid (Winnipesaukee, sol 653) was analyzed for composition, appearing mafic (Fe-rich), in contrast to the relatively felsic host rock. The interior surface of the spheroid appears to have a similar composition to the exterior with the possible exceptions of being more hydrated and slightly depleted in Fe and K. Origins of the spheroids as Martian tektites or volcanic bombs appear unlikely due to their hollow and relatively fragile nature and the absence of in-place clearly igneous rocks. A more likely explanation to both the voids and the hollow spheroids is reaction of reduced iron with oxidizing groundwater followed by some re-precipitation as cemented rind concretions at a chemical reaction front. Although some terrestrial concretion analogs are produced from a precursor siderite or pyrite, diagenetic minerals could also be direct precipitates for other terrestrial concretions. The Gale sediments differ from terrestrial sandstones in their high initial iron content, perhaps facilitating a higher occurrence of such diagenetic reactions.

1. Introduction

The Mars Science Laboratory (MSL) rover, *Curiosity*, is the first to traverse across and explore substantial sedimentary deposits in a depression that was once a large, habitable lake (Grotzinger et al., 2015). The first nine kilometers of the traverse (Fig. 1) covered terrain characterized by conglomerates (e.g., Williams et al., 2013), sandstones (e.g., Anderson et al., 2015), and mudstones (e.g., Grotzinger et al. 2014; McLennan et al., 2014). Evidence from the morphology (Grotzinger et al. 2014) as well as the chemistry and mineralogy (e.g., Vaniman et al., 2014) point towards deposition of much of the material in either flowing water or in a significant body of standing water. Further, the rover team's observation of dipping beds interpreted as foresets occurring over a significant fraction of this traverse suggests that a large sediment load was deposited over an elevation of at least 200 m (Grotzinger et al., 2015). The amount of sediments suggests that the lake, or succession of lakes, was long-lived, likely existing a minimum of 10,000 to as much as 10 million years or more, as a large standing body of water (Grotzinger et al., 2015; Palucis et al., 2016).

Observation of the surface texture at Yellowknife Bay revealed areas covered with millimeter-scale nodules concentrated most strongly over and around the Cumberland drill site but also near the John Klein drill hole. A total of 1729 solid nodules and 513 hollow nodules were measured in 20 Mars Hand Lens Imager (MAHLI) images of the surface in this area (Stack et al., 2014). The nodules were suggested to have originated as concretions, possibly surrounding gas bubbles (Grotzinger et al., 2014; Kah et al., 2014). No compositional differences were detected by ChemCam in the nodules compared to the average Sheepbed unit composition, except when filled by calcium sulfate, which is interpreted as a late stage filling of a pre-existing cavity (Nachon et al., 2014).

In this work we study larger post-depositional features, specifically hollow spheroids up to ~23 cm in diameter, interpreted as concretions, and spheroidal voids in the ~1-10 cm range in nearby bedded material. Collectively these features may provide further clues to diagenetic processes in the Gale crater sediments.

2. Methods

Features were imaged mostly by the Mastcam instrument, consisting of stereo cameras mounted on the rover's mast. These are variable focus, fixed aperture color cameras employing identical CCDs with 1600 x 1200 pixels. The two have longer and shorter focal lengths to simultaneously capture higher resolution and larger fields of view. The left camera has a 34 mm focal length, a 0.22 mrad/pixel resolution, and an 18.4 x 15 degree effective field of view. The right-side camera has a 100 mm focal length yielding a 0.074 mrad/pixel resolution, and an effective field of view of 6.3 x 5.1 degrees. Both use Bayer red-green-blue filters for all images, in addition to a color filter wheel that is optionally used (Malin et al., 2010; Bell et al., 2012). One image used in this work was taken by the MAHLI camera on the rover arm. It is designed for both close-up and distant imaging using the same detector and Bayer color filter as Mastcam (Edgett et al., 2012). Imaging of the Winnipesaukee target was also done by the ChemCam Remote Micro-Imager (RMI). This camera images through the 110 mm diameter ChemCam telescope using a flight-spare Rosetta camera head. The RMI takes panchromatic images that are weighted somewhat toward the longer-wavelength region allowed by silicon CCDs (Maurice et al., 2012). The RMI has a 20 milliradian field of view; its pixel resolution is 19 microradians, however, its resolution

is not pixel-limited, as the telescope was designed to also accommodate the compositional analyses, with a resulting effective resolution of ~40 microradians (Le Mouélic et al., 2015).

Compositions described for the Winnipesaukee target were obtained with the ChemCam Laser-Induced Breakdown Spectrometer (LIBS) instrument. The LIBS technique obtains elemental compositions by firing a focused laser pulse onto a small spot on a target to ablate material producing a hot (~10,000 Kelvin) plasma. The plasma is imaged and the light is spectrally dispersed to observe optical emission lines of the ablated material (e.g., Cremers and Radziemski, 2006). The ChemCam LIBS instrument covers the spectral range from 240-906 nm, observing plasmas to a distance of 7 m (Wiens et al., 2012; Maurice et al., 2012). The LIBS footprint is ~400 μm at the distance from which Winnipesaukee was observed. Observations into soil produce a somewhat larger hole with a diameter of 1-1.5 mm. For each observation point, 30 laser pulses were used, with a corresponding spectrum recorded for each. Reported compositions usually discard the first five spectra and average the remaining 25, but compositions corresponding to each laser pulse can be determined if depth-sensitive information is desired.

ChemCam LIBS spectra are processed to remove noise, ambient light, and white-light continuum (Wiens et al., 2013). The major-element abundances are determined using a combination of two multivariate techniques, partial least squares (PLS; e.g., Anderson et al., 2017) and independent component analysis (ICA; e.g., Forni et al., 2013), based on calibration with over 400 standards in the laboratory, cross correlated with Mars observations via comparison of eight geological standards on the rover (Clegg et al., 2017). This calibration has been shown to give results in good agreement with the Alpha Particle X-ray Spectrometer (APXS) and with precision within a factor of ~2 of that instrument (Clegg et al., 2017).

ChemCam LIBS provides qualitative assessments of hydrogen abundances via an emission line at 656.8 nm (Schroeder et al., 2015). On the other hand, the elements sulfur, chlorine, and phosphorous are poorly constrained by ChemCam and are thus not generally quantified. The totals of the quantified elements are usually below 100 wt. % due to the fact that S, Cl, P, and H generally comprise a small to moderate fraction of the total abundances. The sum of these 'missing elements' can often be inferred by the difference between the ChemCam major-element total and 100 wt. %.

3. Field Area Description

The features described here were observed on sol 121-123 (Tochatwi and nearby features), sols 302-305 (Point Lake Outcrop, and Shaler a few sols later), sols 343-345 (Twin Cairns Island), and sol 653 (Winnipesaukee). Figs. 1 and 2 show the locations of these features. Bradbury Rise is a relatively flat area at the distal end of the alluvial fan produced by the Peace Vallis flow channel (Palucis et al., 2014) that extends down from the wall of the crater ~20 km northwest of the landing site. Bradbury Rise is bounded (white dashed line, Fig. 1) on the south-southeast by the Bagnold Dune field and the lower slopes of Mt. Sharp. Along the rover's traverse it extends from near Yellowknife Bay (YKB) on the northeast, to north of Kimberley, where the rover began to encounter shallow valleys, buttes, and mesas. The surface of Bradbury Rise is characterized by sedimentary gravel and occasional conglomerate outcrops in three different types of surface expression: Hummocky Plains, Cratered Surface (CS), and a Rugged Unit (Fig. 1), although the rover never actually drove on the CS unit. To the east of the landing site is a

triple junction between the Hummocky Plains, a CS unit, and a region of relatively high thermal inertia at YKB (Fig. 2). A number of the spheroidal features discussed in this work were found in this area, including Tochatwi and features at Point Lake and Shaler (Fig. 2).

The YKB formation consists of three different members described in Grotzinger et al. (2014): Sheepbed, Gillespie, and Glenelg. The lowest member, Sheepbed, consists of mudstones. In addition to the nodules and raised ridges, this member is characterized by significant calcium sulfate veins and small nodules (Nachon et al., 2014). Sheepbed was sampled by CheMin and SAM in two different drill holes, both of which yielded clay minerals as well as primary detrital basaltic grains. The CheMin analyses show 18-22% smectite, along with several percent abundances of magnetite, suggesting authigenesis (Vaniman et al., 2014; Bristow et al., 2015; Bridges et al., 2015).

The Sheepbed member is overlain by the Gillespie member, which consists of sandstone of similar composition and hydration (Mangold et al., 2015). By contrast to the lower members, the overlying Glenelg member appears to encompass a diversity of materials and surface expressions. The Rocknest outcrop contains rocks of two different morphologies, both of which are enriched in FeO_T (> 25 wt. %) and depleted in MgO (Blaney et al., 2014; Mangold et al., 2015). These differ from nearby Bathurst outcrop which is rich in magnesium and potassium (Mangold et al., 2015). Closer to Gillespie and Sheepbed, the Point Lake outcrop appeared chemically to be intermediate between Rocknest and the underlying Gillespie and Sheepbed units. About 30 m south of Point Lake, the Shaler outcrop is interpreted as cross-bedded fluvial sandstones and interbedded mudstones characterized by a distinctive platy weathering morphology (Anderson et al., 2015; Grotzinger et al., 2014).

From YKB the rover drove southwest (Fig. 1), back across the Bradbury Rise. Curiosity entered a region of valleys and mesas (Stack et al., 2016; Williams et al., 2016) starting about 1 km northeast of Kimberley. After leaving the Kimberley, the terrain was once again relatively level until the rover passed the landing ellipse boundary and briefly entered Hidden Valley. While most of the objects described in this paper were encountered near YKB, another spheroidal feature, Winnipesaukee, was found by Curiosity on sol 653 at an elevation of -4477 m, 600 m southwest of Kimberley and ~6 km from YKB. Fig. 1 shows the region around Winnipesaukee mapped as Hummocky Plains (e.g., Grotzinger et al., 2015).

The objects described here were serendipitously observed and sampled while other priorities were being addressed. The rover was on a strict schedule to arrive at selected destinations and waypoints. In mapping a terrestrial field area, features can be observed and mapped comprehensively over days, allowing time to find the best examples of various features. However, on rover missions in general, and especially during this part of the MSL mission, we are only able to study features that happened to appear in images, and for which the team had enough time to react to request analyses or additional imaging.

4. Results

4.1. Tochatwi

On sol 121 Curiosity imaged the first hollow spheroid, Tochatwi (Fig. 3), as it was driving away from its first encounter with the Shaler outcrop on its way to the Sheepbed member (Fig. 2). The

material around Tochatwi appears to be relatively flat, weathered sandstone of the Glenelg member with relatively thin dust covering. Several circular objects were observed to protrude from the sandstone surface in the vicinity of Tochatwi. Two objects were observed on sol 123 (Fig. S1b, c in supplementary materials). One of these is directly adjacent to a ChemCam observation of a target named Kahochella. Both of these two circular objects have rough exterior surfaces and it was not clear if these features are spheroidal or if they are cylindrical, possibly sedimentary pipes (Rubin et al., 2016).

By contrast, Tochatwi clearly appears spherical. However, given that only a portion is visible above the bedrock, the actual shape could be like that of a blister (height less than horizontal diameter). The protruding portion is ~16 cm in diameter. The ground appears to intersect the shell at an interior angle of approximately 45°, implying that if the subsurface continuation of this feature is spheroidal, its diameter is ~23 cm. (Here the term "shell" is used to describe the physically resistant, outer rind of the spherical feature and does not imply any biogenic significance.) The shell is darker than the surrounding sandstone. Other than the Mastcam Bayer filter color, there is no further information on its spectral or compositional properties, as ChemCam was not used on this target. Closer inspection of the feature (Fig. 3b) indicates that the walls have somewhat variable thickness in the range of 1-4 mm. A portion of some remaining material from the inside is visible in the upper left side of the object, clearly containing voids of variable sizes up to 2 mm in diameter (Fig. 3c). Several small, millimeter-size voids can also be seen on the outer surface of the shell. The outer surface appears relatively smooth; it may show some scalloping on the right side, but this could be due to aeolian erosion. As the spheroid walls protrude from the surrounding rock, it can be assumed that their cohesiveness is greater than that of the surrounding sandstone. This cohesiveness is also needed to explain how an object this thin is not more easily weathered or broken.

4.2.Point Lake, Shaler, and Twin Cairns Island Features

After completing analysis of the Sheepbed mudstones, Curiosity visited the Point Lake outcrop on sols 302-305 before returning to the Shaler outcrop. Point Lake (Fig. 2) was observed in the distance as early as sol ~63, as it protrudes ~50 cm above the Gillespie member. Point Lake was noted by Grotzinger et al. (2014) to be vuggy. Fig. 4 shows a portion of the outcrop displaying its rough texture with vugs up to ~3 cm in diameter. To the right, under an overhanging portion of the outcrop and just at the contact, an ovoid feature appears to be poorly anchored to the outcrop. An inset shows the feature from a slightly different angle, and shows a number of spheroidal shell fragments still attached to the outcrop to the left and right of the main feature. Additional fragments lie on the ground or are partially buried just below the outcrop. The main feature is ~ 10 cm in diameter, whereas the fragments appear to be from objects closer to 5 cm original diameter. The larger feature is fractured with some light-toned material comprising a portion of the interior. Overall, the spheroidal feature appears lighter-toned than the Point Lake outcrop but as dark as or somewhat darker than the Gillespie member surface just below the outcrop. The location of this feature below the dark-toned outcrop resulted in relatively low lighting for the images. The slope of the surface just below the outcrop also made it difficult to position the rover for closer imaging with the arm-mounted MAHLI, which imaged nearby surfaces of the outcrop (Grotzinger et al., 2014).

The Shaler outcrop, ~40 m from Point Lake (Fig. 2), consists of alternating recessive and resistant sandstone layers (Anderson et al., 2015). Shaler lies stratigraphically above the Point

Lake outcrop (Mangold et al., 2015) and at the base of Shaler are some highly pitted layers. Mangold et al. (2015) noted that the pitted layers of Shaler bore a strong compositional resemblance to Point Lake, with a depletion of Mg in both. The Shaler pitted layer (Fig. S2) displays the same spheroidal void structures as observed in Point Lake, and one hollow spheroid with a diameter of ~50 mm was observed in an image of a pitted surface nearby (Fig. S3). Another object was observed on sol 308 (Fig. S4) in the vicinity of Shaler. This one may have been a hollow spheroid or it may be the remnant of a sedimentary pipe (Rubin et al., 2016). A notable feature is the "Swiss cheese" texture with centimeter-size holes in the otherwise smooth-looking walls. These vugs may be larger versions of the small voids seen in Tochatwi.

On sol 343-345, at a distance of ~0.5 km from Point Lake, the rover passed near and imaged an outcrop named Twin Cairns Island (Fig. 5). Mastcam images taken from a distance of 45-50 m show that this outcrop contains numerous (e.g., more than eight) spheroidal voids that are partially exposed within the outcrop. The larger of these voids are 2.5-3 cm in diameter, similar in size to those observed at Point Lake. The Twin Cairns Island outcrop and several other local topographic highs on Bradbury Rise were originally mapped as the "rugged unit", distinct from the Yellowknife Bay members and from the Cratered Unit (Jacob et al., 2014). However, the dark texture and voids in this outcrop suggests a strong similarity to Point Lake.

4.3.Winnipesaukee

Another hollow spheroid, Winnipesaukee, encountered on sol 653 (Wiens et al., 2015), is shown in Fig. 6. This spheroid is embedded within a light-toned rock matrix that is exposed above the gravelly surface over a diameter of ~35 cm. A number of other clasts appear to be protruding above the weathered matrix surface, some featuring vugs. Rock exposures of similar appearance occur nearby. Two other ChemCam targets, Meetinghouse and Albee, were also observed on sol 653. Meetinghouse is similarly light-toned as the Winnipesaukee host rock. Its upper surface is weathered flat but rough and the few visible clasts are much smaller and lighter-toned than those in the Winnipesaukee host. The RMI image of Albee (not shown) has a much different appearance. This clast is partially buried in the gravelly fill but the upper part protrudes higher than the other two rocks. The clast is somewhat darker in appearance and the RMI image shows distinct coarse crystals, indicating that this is a partially buried igneous float, not related to the other two. Another image taken at the Kimberley outcrop (600 meters away; Fig. 1) on sol 597 shows what appears to be small hollow spheroids, potentially showing a transition in morphology between voids and hollow spheroids (Fig. S5). Additionally, on a topographic rise imaged one sol after Winnipesaukee, darker-toned, somewhat vesiculated boulders were observed that appear similar to those at Point Lake and Twin Cairns Island.

The spheroidal Winnipesaukee object is dark-toned, appearing roughly similar to Tochatwi, with a similar shell thickness, but overall it is significantly smaller, at 2.5-3 cm diameter. Some small protrusions may indicate weathered small voids. Small light-toned grains, 0.5 mm and smaller, occur throughout the object's dark surface. The spheroid is hollow with the exception of soil that is likely aeolian in nature.

Winnipesaukee is the only one of the three large hollow spheroids that was analyzed for chemical composition. ChemCam performed a 1x10 line scan across the spheroid, the locations of which are shown in Fig. 6. Table 1 gives the compositions of the individual points along the scan, which covers the bedrock at each end, the exterior of the spheroid, and soil lying inside the

spheroid. Points 1, 9, and 10 sampled the host rock and have felsic compositions, including SiO_2 > 50 wt. %, (Na_2O+K_2O) > 7 wt. %, MgO < 2 wt. %, and FeO_T < 8 wt. %. Points 2 and 3 show relatively similar compositions possibly having targeted the host rock, but at least one of these might have hit a pebble instead of the host rock according to the image in Fig. 6b. Points 6, 7, and 8 hit the top of the spheroid, and their compositions reflect more mafic compositions, with SiO_2 < 55 wt. % and FeO_T 14-20 wt. %. Calcium is still variable, and the alkali elements are still relatively high. Two points (4 and 5) sampled inside the spheroid, hitting soil. These show the high hydrogen signal typical of fine-grained soil (Fig 6c; Schroeder et al., 2015; Cousin et al., 2015), higher MgO, and relatively low SiO_2 and K_2O.

In order to see the trends better, the points representing each surface—host rock, soil, and spheroid—were averaged together in Table 2. The standard deviations of these means, as well as the precision of the shots (Table 1) are much smaller than the differences between these features for most elements. The mean composition of the host rock is nearly the same as the nearby rock, Meetinghouse, which was also observed by ChemCam. Both are clearly felsic in composition. By contrast, the exterior of the Winnipesaukee spheroid is well within the olivine-normative portion of the silica range, quite different from the host rock. The compositions of points 6, 7, and 8 indicate some chemical heterogeneity of the outer surface of the spheroid, as the differences are well beyond the precision observed within a raster (Blaney et al., 2014).

Trace elements Li, Rb, Sr, Ba, and Cu were also quantified from the LIBS spectra, as described in Payre et al. (2016a, b). Abundances of these elements are generally unremarkable with the exception that the average Li abundance in points 6-8 (exterior of spheroid), at 18 ppm, is ~50% higher than the average of points 1, 9, and 10, representing the host rock. In general the points that sampled the exterior of the spheroid are significantly lower in Sr (< 200 ppm) and Ba (<150 ppm) than the more felsic compositions of the points that sampled the host rock, though there is substantial scatter. Point 9 in particular is enriched in these elements, with > 700 ppm Sr and > 600 ppm Ba.

The inside of the Winnipesaukee spheroid was targeted by LIBS points 4 and 5. The RMI image (Fig. 6b) shows that this area was partially filled with soil, as mentioned above. However, analysis of the individual-shot trends for points 4 and 5 reveals additional detail. All thirty shots of point 5 resulted in similar spectra. However, in point 4 the composition changes significantly, starting around shot number nine. This is seen most clearly with magnesium, shown in Fig. 7, where the MgO drops from ~7 wt. %, typical for soil, to a value of around 4 wt.%. The trend is given for all of the major elements in Table 2, where the last ten shots are averaged and compared with the first ten shots (the first five spectra were not removed as is normally done to avoid dust on rocks) from both points 4 and 5. Silica, Al_2O_3, Na_2O, and K_2O increase significantly, while FeO_T decreases and CaO shows a slight increase. Some of these trends are consistent with the composition of the spheroidal shell, as if the laser had sampled an interior portion of the shell, but several element trends are inconsistent with that. In particular, the decrease in Fe and increase in Al and Ca are different. In addition, SiO_2 increases above the level of the exterior of the shell, and Ti drops more than expected. Finally, the 656 nm hydrogen peak in the LIBS spectra, indicated in Fig. 6, shows quite strong hydration. These results are discussed below.

The spectrometers on ChemCam are also used in passive mode to record visible/near-infrared (400-840 nm) radiance from the martian surface. Such observations typically are acquired as

"darks" by ChemCam after laser shots to assist in calibration of LIBS measurements. Johnson et al. (2015, 2016) used onboard calibration targets as reflectance standards to reduce the passive radiance observations of sunlit targets to relative reflectance. Most of the spectra that were collected exhibit a ferric absorption edge in the visible region (< 600 nm) and maximum reflectance values near 0.25, typical of dusty martian soils. Figure 8 shows such spectra from Winnipesaukee (Sol 654) where three spectrally distinct materials are apparent. Locations with relatively high Si values (#1, 2, 3, 9, and 10) within the light-toned host rock show maximum relative reflectances of 0.20-0.25. Locations #4-5 on nearby soils exhibit lower relative reflectance values. Similarly low values occur for locations #6-8 on the spheroidal feature itself, consistent with a less dusty surface. These locations also exhibit flatter spectra (less spectral contrast) and negative slopes toward the near-infrared, with peak reflectances near 600 nm. This is consistent with the more mafic elemental chemistry determined from the LIBS measurements, as would be expected from a stronger presence of magnetite, for example.

5. Discussion

5.1. Relationship to Host Rock

The Winnipesaukee spheroid has a substantially different composition from the host rock. As the other large hollow spheroids—Tochatwi and the one at Point Lake—were not targeted with ChemCam, it is impossible to know if their compositions are the same as Winnipesaukee. However, the objects observed earlier are embedded in a darker-toned mudstone, so their appearance is more similar to the host rock than Winnipesaukee is to its host rock. The Winnipesaukee host rock appears more as a conglomerate, rather than a sandstone. Given the difference in host rocks, in contrast to the similar, dark appearance of the hollow spheroids, it is possible that Winnipesaukee was transported and not formed in place.

5.2. Relationship to Nodules and Mini-bowls

Nodules and hollow or collapsed nodules referred to as "mini-bowls" were observed in abundance in certain areas of the Sheepbed member (Stack et al., 2014). The size distributions of the nodules in that study were all <1 cm diameter. Nodules were not limited to the Sheepbed member. Nodules also existed in a sedimentary dike feature (Fig. 9) referred to as the snake, after a target named Snake River (Grotzinger et al., 2014). Here again, these nodules were generally < 1 cm in diameter. Nodules were also observed along several more recent parts of the rover traverse, including in portions of the Pahrump outcrop (sols ~750-900) and in the Stimson unit (sols ~1150-1280). The latter is an aeolian sandstone that unconformably overlies previously-deposited and eroded material (Grotzinger et al., 2015). Pahrump is part of the Murray formation (Grotzinger et al., 2015), which is observed from orbit over a number of kilometers on the lower portions of Mt. Sharp. Rover observations suggest it is a lacustrine deposit but with significantly different composition from the Sheepbed mudstones, being enriched in aluminum and alkali elements, and variably depleted in Mg (Forni et al., 2015; Blaney et al.; 2015).

The images of voids and hollow spheroids at Point Lake (Fig. 4), just a few meters from the Sheepbed Member, suggest a possible link between the < 1 cm nodules found in great abundance there and the larger spheroids discussed here. The inset in Fig. 4 shows partially intact spheroidal shells (discussed later) with diameters as small as 2-4 cm, not much larger than the nodules.

5.3. Interior of Winnipesaukee

Probing the chemistry of the interior surface of the Winnipesaukee shell potentially provides additional information relating to its origin. From descriptions at the end of Section 4.3, it is clear that that the last 20 laser shots of observation point 4 encountered a solid material of different composition from the soil seen in the image. The shot-to-shot behavior of the LIBS signal gives a strong indication that these spectra interrogated a solid surface. Cousin et al. (2015) noted that the total emission (sum of the signal in all channels) observed from fine-grained soil is variable from shot to shot. However, when a solid object is observed, the total emission becomes much more stable. The same behavior is observed here. One possibility is that this solid material is the interior surface at the bottom of the spheroid. If that is the case, the differences in composition from the exterior wall of the spheroid, pointed out in Section 4.3, may provide information about the interior surface, and possibly about the original contents of the spheroid or its formation mechanism. However, in inspecting the differences—higher Al_2O_3 and CaO, and lower FeO_T and K_2O—the only general implication is that the interior seems slightly more felsic or less mafic than the exterior. One other possible clue is the high hydration signal, possibly suggesting the addition of hydrous phases such as clay minerals or a hydrated cement.

High hydrogen was also observed in an apparent sedimentary pipe targeted by ChemCam on sol 530 and called Tappers (Rubin et al., 2016). The pipe, located ~1 km away, had one of the highest hydrogen signals of all the solid objects observed along the traverse. However, Tappers is high in iron (> 20 wt. % FeO_T) and also Mg (> 10 wt. % MgO) and is relatively low in aluminum and alkali elements. It may contain Fe-Mg smectite or serpentine, given the apparent high water content.

5.4. Origin of Hollow Spheroids

Terrestrial sandstone formations are known to contain features of many different morphologies including concretions, arches, doughnuts, and pipes (e.g., Young et al., 2009). Terrestrial spheroidal concretions are diagenetic, cemented mineral masses that can have a variety of cement precipitates such as iron oxides and calcite (e.g., Berner, 1968; Raiswell, 1971; Chan et al., 2012). Due to their greater hardness, the concretions appear as surface lag after the less cemented surrounding sandstone weathers away. An important characteristic of the concretions is that the cement precipitate causes the concretion itself to be mineralogically and often also chemically distinct from the host rock. Although most occurrences of terrestrial concretions are small (< 1 cm diameter), large iron oxide concretions of > 10 cm diameter occur in Jurassic Navajo sandstones (e.g., Chan et al., 2012).

Concretions have also been seen on Mars, not only on the MSL mission (Stack et al., 2014), but also at the Opportunity rover landing site in Meridiani Planum (“blueberries”), where they consist of pure hematite and are < 5 mm diameter (Squyres et al., 2004; Grotzinger et al., 2005; Arvidson et al., 2014). Opportunity also identified some small hollow spheroids of the same general size as the blueberries, distributed both in loose soils atop the Hesperian Burns formation and tightly embedded in bedrock on the highest reaches of the Noachian Matijevic Hill (Fairén et al., 2014).

Larger and hollow features have also been encountered by the previous generation of rovers. The Spirit rover encountered a large spherical exfoliation feature on sol 103 of its mission (Fig. S6). This feature is > 33 cm in diameter and is heavily weathered, but it clearly appears to be solid

and not hollow. Some rocks encountered later at the edge of the Bonneville ejecta deposit (foreground of Fig. 7, Arvidson et al., 2006) and at the foot of Columbia Hills (MER-A, sols ~160-180) have highly weathered and easily eroded interiors surrounded by resistant shells, - a feature generally referred to as *case hardening* (Arvidson et al., 2006 and references therein; Crumpler et al., 2011; Fig. S7). These rocks are partly hollow like the features described here (e.g. Tochatwi, Winnipesaukee), but do not have a spherical shape. Overall, the Gale crater hollow spheroids are significantly different from previously observed features on Mars due to their composition (not hematite concretions), their size, strikingly spherical shape, and their hollow nature.

The following discussion highlights possible interpretations of the cm- to dm-size hollow spheroids in Gale crater, and why a concretion origin seems most consistent with these features.

Igneous origin: Stack et al. (2014) concluded that the nodules found in the Sheepbed Member were not likely to be of igneous or impact origin, favoring instead an explanation as authigenic mineralization precipitated from diagenetic pore fluids. The large spheroids discussed here could not be volcanic bombs, which are ballistic pyroclasts with a diameter > 64 mm, or lapilli (smaller pyroclasts). These are masses of molten (and fragmented) rock, which have an (approximately) aerodynamic shape during flight, and depending on cooling status, deform, crack and break apart upon landing. Some contain vesicles, especially in a glassy rind, but bombs are not normally hollow (e.g., Macdonald, 1972; Schmid, 1981; Blong, 1984; Gurioli et al., 2013). Smaller ejecta are classified as lapilli, and can consist of scoria, rock fragments or magma clots. Although frequently vesicular, completely hollow volcanic spheroids would not survive the landing impact and are therefore generally not normally preserved (Schmid, 1981, Blong, 1984).

Meteorite impacts: Meteoritic impacts produce molten ejecta called tektites. They are generally spherical to tear-drop-shaped objects formed from melt material that solidifies during passage through the atmosphere following a large impact (e.g., Stöffler and Grieve, 2007; Stauffer and Butler, 2010); they can fall many kilometers from their origin. Mars is likely to also produce tektites, particularly if its atmosphere was thicker during the late heavy bombardment period. The rate of impacts on Mars is likely to have been much higher at the time of the formation of the Gale crater sediments (e.g., Carr and Head, 2010), suggesting that tektites might be quite numerous in sediments of this age. One potentially dubious suggestion for the origin of the Meridiani blueberries was as cosmic spherules, which are also produced from impacts (Misra et al., 2014). By contrast, Martian tektites would reflect the local composition of their place of origin, so their composition might not differ significantly from the fine-grained sediments in Gale crater. Hollow tektites are known to occur on Earth. The gas-bubble interior can comprise a relatively large fraction of the overall volume of the object, with interior volumes of up to 50 cm^3 reported (Baker, 1965). The overall morphology and shape of Winnipesaukee could be similar to that expected for a hollow tektite. However, the morphologies of other objects described here are not consistent with tektites. The thin walls of Tochatwi and its overall size and aspect ratio do not seem consistent with an origin as a tektite, and the multiple shells and voids at Point Lake clearly do not fit this hypothesis.

Gas or fluid bubbles: The thin walls, large aspect ratios, and the apparent relationship between voids and hollow spheroids and fragments at Point Lake suggest a possible origin as gas or fluid bubbles within sediments prior to solidification. Such bubbles could come from the inorganic reaction of mafic minerals, especially olivine, to serpentine (e.g., Oze and Sharma, 2005), the

degradation of organic material, or fluctuations in lake level that cause air to enter the sediment when lake level is low and then be trapped as bubbles within the sediment when lake level rises. Gas bubbles have been inferred in terrestrial ancient lacustrine sediments that display "molar tooth structure" in which gas-produced voids were filled and preserved by Ca sulfate (Grotzinger et al., 2014 and references therein). Gas-produced voids have been found in modern terrestrial lacustrine sediments, for example in the Lake Powell delta (Simpson et al., 2016). These voids are not limited to orienting along bedding planes. If mineralization occurs early enough, the structure may be maintained. *Curiosity* investigations found small amounts of olivine (2.8 and 0.9%, respectively) in the John Klein and Cumberland drill holes in the Sheepbed mudstone, alongside 22% and 18% smectite (Vaniman et al., 2014). If the Rocknest sand shadow, with 16% olivine (Vaniman et al., 2014), is assumed to be a potential unaltered precursor of the Cumberland and John Klein samples, reaction pathways from this starting material to the observed 'mudstones' would favor the dissolution of olivine (Bristow et al., 2015) and the XRD-amorphous component (Bridges et al., 2015), potentially forming gas in the process. Additionally, the SAM instrument detected small amounts of carbon compounds in the Yellowknife Bay samples, which have the potential to release gas (CO_2, CO; Ming et al., 2014; Eigenbrode et al. 2014; Freissinet et al. 2015). Thus, a gas or brine-gas mixture in the voids could provide a chemical and/or redox gradient necessary for the localized formation of secondary minerals along the boundary between the void and the sediment.

Redox gradients: Alternatively, such a chemical gradient could be sourced from alteration of a chemically reducing precursor mineral, e.g., a sulfide or carbonate. According to Loope et al. (2012), hollow, rinded concretions form on Earth when siderite, either formed in place or transported fluvially a short distance, is dissolved, liberating ferrous iron which diffuses to the perimeter of the structure. Ferrous iron is oxidized by dissolved oxygen to precipitate ferric oxyhydroxide minerals. Precipitation of these minerals generates acid that leads to further dissolution. Loope et al. (2012) argue that the precursor siderite concretion is thus altered by oxidative processes to form a thick Fe-oxide rind with a hollow interior. 'Rattlestones' found in the Netherlands are attributed to a similar two-step process, whereby Fe-oxides replace a pre-existing siderite concretion, leaving a void (e.g., van der Burg, 1969). Other hollow concretions have been found to have siderite walls (Marza et al., 2004).

Perhaps the most relevant terrestrial analog in terms of morphology and chemistry invokes reactions of pyrite mineral(s) in sediments that undergo alteration and oxidation to form hollow spheroidal clasts. Hollow spheroidal clasts associated with pyrite cores found in sandstones in Surrey, England, were reported by Smith (1957). More spectacular examples, up to 60 cm in diameter, are found in the Khorat Group in northeastern Thailand (Putthapiban and Hongsresawat, 2007). Some of the spheroids have small remnants of pyrite inside them. It is proposed that pyrite nodules were deposited in fluvial sediments and bedded silt, and that interaction with water resulted in a reaction front in which an enriched Fe^{2+}/Fe^{3+} solution percolates outward until the system reaches equilibrium. The iron-enriched sediment hardens, cementing the sediments at the reaction front. Figure 5a of Putthapiban and Hongsresawat (2007) looks remarkably like the Point Lake and Twin Cairns Island morphology, with numerous voids of various sizes, along with hollow spheroids. One of the Point Lake voids contains apparent remnant material (Fig. 10; the location of this void relative to the spheroidal shells in Fig. 4 is shown in Fig. S8). However, this apparent filling material was not analyzed for composition, and thus it is not possible to conclude anything on its content.

These terrestrial examples generally result in hollow concretions consisting of iron oxides or carbonates, which contrasts with the iron-rich silicate composition of the Winnipesaukee spheroidal shell. Additionally, although some siderite is inferred to have been found on Mars by the Spirit rover (Morris et al., 2010), and the possible presence of trace amounts of carbonates in Gale sediments may have been the source of some CO_2 observed by SAM (Eigenbrode et al. 2014; Freissinet et al. 2015), it was not identified among the mineral constituents of the Sheepbed Mudstones (Vaniman et al., 2014). On the other hand, the mudstones clearly contain reduced iron, with significantly more magnetite (~4%) than hematite (< 1%). The CheMin team also reported > 1% abundances of akaganeite, and found pyrite near the limit of detection in the John Klein sample (Vaniman et al., 2014). The Windjana drill hole at the Kimberley, near the Winnipesaukee location, does not contain observable pyrite, but it contains 12% magnetite, along with only 0.6% hematite and 0.3% pyrrhotite, so the iron is in a relatively low oxidation state (Treiman et al., 2016).

On Earth there are a wide range of iron oxide concretions with different morphologies and mineralogies, and complex histories of fluid flow. Besides the terrestrial examples of concretions mentioned above, there is evidence that some terrestrial Fe-rich concretions may not require siderite or sulfides to form. Hydrous ferric oxide concretions are proposed for Jurassic Navajo Sandstone of Utah, USA, where macroscopic rind concretions show multiple generations of cement with different textures, and some with a hardened outer shell and a weakly cemented interior (Potter and Chan, 2011; Potter et al., 2011). Scanning electron microscope images show the infilling of the Fe-rich material in the pores of the sandstone (Potter et al., 2011). Trace-element studies of the concretions reveal enrichments of U. Since U would be mobilized by an oxidizing fluid required to produce the concretions from a reduced iron species, its presence suggests instead that the iron oxide/oxyhydroxide was an original precipitate (Potter et al., 2011).

Passive spectra of the Winnipesaukee target show a ferric absorption edge (Section 4.3; Fig. 8), but unaltered host rock minerals contain ferrous iron, which also is the more readily mobile Fe species. This provides evidence for a redox gradient, which is one possible driving force for the localized formation of secondary alteration phases. It therefore seems plausible that redox changes could lead to the localized formation of secondary phases, changing the oxidation state from Fe^{2+} to Fe^{3+}. We therefore feel justified in classifying these spheroidal features as concretions.

Raiswell and Fisher (2000) describe two growth mechanisms for concretion development: either concentrically, in which the feature's radius grows over time, or pervasively, in which an isolated patch of crystals evolves toward a mass of zoned crystallites. In the latter case the radius does not grow, but pore space is filled. A combination of these mechanisms may also occur, in which pervasive growth may be followed by concentric growth, with a concomitant change in the nature of the cementing material. To explain hydrous ferric oxide (HFO) concretions found in eolian Jurassic Navajo Sandstone in the southwestern United States, Potter et al. (2011) use a pervasive growth model in which amorphous HFO is precipitated in localized concentrations and pore spaces are later filled in, with cementation proceeding inwards from the outer edge, or rind. Studies of thin sections by scanning electron microscope appear to confirm the inward growth. While we cannot study the martian hollow spheroids with such detail, the apparent iron-rich nature of the features is consistent with the possibility of an iron-rich cement filling the pore spaces to create an inward-growing shell, in which the interior was not hardened due to the

chemical barrier created in the process. As a result, the system runs out of reactants, so the case cementation cannot continue filling in.

In contrast to terrestrial sandstones which are generally highly silicic, sandstones in Gale crater are relatively iron-rich, at nearly 20 wt. % FeO_T, and this is likely true for much of Mars' sandstones. Because iron is freely available, the role of redox reactions involving iron as a major constituent of the martian sediments is apparently much stronger in terms of producing secondary alteration within the sediments. On Earth the abundance of organic materials as well as the oxidizing nature of the terrestrial atmosphere play significant roles in redox conditions of near-surface materials. It seems that, by contrast, the agents controlling redox conditions are much less well understood on Mars. Hydrogen and methane (Webster et al., 2014) released by serpentinization reactions (Oze and Sharma, 2005) could be one important factor.

6. Conclusions

We have described unique spheroidal features that have been observed by the Curiosity rover during the early stages of its traverse in Gale crater. The spheroidal shells, with diameters as large as ~23 cm, are most plausibly the product of an alteration gradient from the interaction of groundwater with reduced iron species, possibly in the form of pyrite, iron meteorite fragments, or other forms of reduced iron. If true, these features are additional evidence of the strong role that oxidation plays in diagenesis of martian sediments. The source of the reduced iron is not known at this time. Several possible sources include weathering of olivine, or meteoritic impacts and their products, including the destruction of meteoritic organic material. The hollow spheroids and voids may be related to the smaller nodules (Stack et al., 2014), but this relationship is also currently unknown. Further exploration by *Curiosity* as well as future missions will hopefully further elucidate the findings described here.

Acknowledgements

This work was supported by the NASA Mars Exploration Program in the US, in France by the Centre National d'Etudes Spatiales (CNES), the Institut National des Sciences de l'Univers (INSU), the Centre National de la Recherche Scientifique (CNRS), and the Observatoire des Sciences de l'Univers Nantes Atlantique (OSUNA). Walter Goetz acknowledges support by Deutsche Forschungsgemeinschaft (DFG grant GO 2288/1-1). Alberto Fairén was supported by the Project "icyMARS", European Research Council Starting Grant no 307496. This work was supported by UKSA in the UK. Part of this research was carried out at the Jet Propulsion Laboratory, California Institute of Technology, under a contract with the National Aeronautics and Space Administration. The many scientists and engineers who built and operated the MSL mission are thanked for their part in this work. Data used in this study are available at the Planetary Data System (https://pds.jpl.nasa.gov). James W. Rice, Jr., Planetary Science Institute, Tucson, helped analyze images acquired by Pancam/Spirit for one of the supplementary figures. P. Gasda is thanked for assistance with one image. Two anonymous reviewers are gratefully acknowledged for their comments. SDG.

References

Anderson R.B., Bridges J.C., Williams A., Edgar L., Ollila A., Williams J., Nachon M., Mangold N., Schieber J., Gupta S., Dromart G., Wiens R.C., Le Mouelic S., Forni O., Lanza N., Mezzacappa A., Sautter V., Fisk M., Blaney D., Clark B., Clegg S., Gasnault O., Lasue J., Leveillé R., Lewin E., Lewis K.W., Maurice S., Schwenzer S.P., and Vaniman D. (2015) ChemCam results from the Shaler outcrop in Gale crater, Mars. Icarus, 249, 2-21, doi:/10.1016/j.icarus.2014.07.025

Anderson R.B., Clegg S.M., Frydenvang J., Wiens R.C., McLennan S., Morris R.V., Ehlmann B., Dyar M.D. (2017) Improved accuracy in quantitative laser-induced breakdown spectroscopy using sub-model partial least squares. Spectrochim. Acta, in press.

Arvidson R.E., Squyres S.W., Anderson R.C., Bell J.F., III, Blaney D., Brückner J., Cabrol N.A., Calvin W.M., Carr M.H., Christensen P.R., Clark B.C., Crumpler L., Des Marais D.J., de Souza P.A., Jr., d'Uston C., Economou T., Farmer J., Farrand W.H., Folkner W., Golombek M., Gorevan S., Grant J.A., Greeley R., Grotzinger J., Guinness E., Hahn B.C., Haskin L., Herkenhoff K.E., Hurowitz J.A., Hviid S., Johnson J.R., Klingelhöfer G., Knoll A.H., Landis G., Leff C., Lemmon M., Li R., Madsen M.B., Malin M.C., McLennan S.M., McSween H.Y., Ming D.W. , Moersch J., Morris R.V., Parker T., Rice J.W., Jr., Richter L., Rieder R., Rodionov D.S., Schröder C., Sims M., Smith M., Smith P., Soderblom L.A., Sullivan R., Thompson S.D., Tosca N.J., Wang A., Wänke H., Ward J., Wdowiak T., Wolff M., and Yen A. (2006), Overview of the Spirit Mars Exploration Rover Mission to Gusev Crater: Landing site to Backstay Rock in the Columbia Hills, J. Geophys. Res. 111, E02S01, doi:10.1029/2005JE002499.

Arvidson R.E., Squyres S.W., Bell J.F. III, Catalano J.G., Clark B.C., Crumpler L.s., de Souza P.A. Jr., Fairen A.G., Farrand W.H., Fox V.K., Gellert R., Ghosh A., Golombek M.P., Grotzinger J.P., Guinness E.A., Herkenhoff K.E., Jolliff B.L., Knoll A.H., Li R., McLennan S.M., Ming D.W., Mittlefehldt D.W., Moore J.M., Morris R.V., Murchie S.L., Parker T.J., Paulsen G., Rice J.W., Ruff S.W., Smith M.D., and Wolff M.J. (2014) Ancient aqueous environments at Endeavor crater, Mars. Science 343, doi:10.1126/science.1248097.

Baker G. (1965) External form and structure of some hollow Australites. *Geochim. Cosmochim. Acta 30*, 607-615.

Bell J.F. III, Malin M.C., Caplinger M.A., Ravine M.A., Godber A.S., Jungers M.C., Rice M.S., and Anderson R.B. (2012) Mastcam multispectral imaging on the Mars Science Laboratory rover: Wavelength coverage and imaging strategies at the Gale crater field site. Lunar Planet. Sci. XLIII, 2541. The Lunar and Planetary Institute, Houston, TX.

Berner R.A. (1968) Calcium carbonate concretions formed by the decomposition of organic matter. Science, 159, 195-197, doi:10.1126/science.159.3811.195.

Blaney D., Wiens R.C., Maurice S., Clegg S.M., Anderson R.B., Kah L.C., Le Mouelic S., Ollila A., Bridges N., Tokar R., Berger G., Bridges J., Cousin A., Clark B., Dyar M.D., Ehlmann B., King P.L., Lanza N., Mangold N., Meslin P.-Y., Newsom H., Schroeder S., Rowland S., Johnson J., Edgar L., Gasnault O., Forni O., and the MSL Science Team (2014) Chemistry and texture of

the rocks at “Rocknest”, Gale crater: Evidence for iron-rich cements. J. Geophys. Res., 119, 2109-2131, DOI: 10.1002/2013JE004590.

Blaney D.L., Anderson R., Bridges J., Calef F., Clegg S., Le Deit L., Fisk M., Forni O., Gasnault O., Kah L., Kronyak R., Lanza N., Lasue J., Mangold N., Maurice S., Milliken R., Ming D., Nachon M., Newsom H., Rapin W., Stack K., Wiens, R., and the MSL science team (2015) Chemo-stratigraphy at the Pahrump outcrop and Garden City vein complex in Gale crater using ChemCam. European Planet. Sci. Conf., September, Nantes, France.

Blong, R. L. Volcanic Hazards: A Sourcebook on the Effects of Eruptions, Academic Press, 1984; Printed in Australia.

Bridges J.C., Schwenzer S.P., Leveillé R., Berger G., Westall F., Wiens R.C., Mangold N., Schmidt M.E., Berger G., and the MSL Science Team (2015) Fluid composition and low temperature alteration at Yellowknife Bay, Mars. J. Geophys. Res. Planets DOI: 10.1002/2014JE004757.

Bristow T.F., Bish D.L., Vaniman D.T., Morris R.V., Blake D.F., Grotzinger J.P., Rampe E.B., Crisp J.A., Achilles C.N., Ming D.W., Ehlmann B.L., King P.L., Bridges J.C., Eigenbrode J.L., Sumner D.W., Chipera S.J., Moorokian J.M., Treiman A.H., Morrison S.M., Downs R.T., Farmer J.D., Des Marais D., Sarrazin P., Floyd M.M., Mischna M.A., MacAdam A.C. (2015) The origin and implications of clay minerals from Yellowknife Bay, Gale crater, Mars. Am. Mineral. 100, 824-836.

Carr M.H. and Head J.W. (2010) Geologic history of Mars, Earth Planet. Sci. Lett. 294, 185–203.

Chan M.A., Potter S.L., Bowen B.B., Parry W.T., Barge L.M., Seiler W., Peters E.U., and Bowman J.R. (2012) Characteristics of terrestrial ferric oxide concretions and implications for Mars. SEPM Special Publication 102, ISBN 978-1-56576-313-5, 253-207.

Clegg S.M., Wiens R.C., Anderson R.B., Forni O., Frydenvang J., Lasue J., Cousin A., Payré. V., Boucher T., Dyar M.D., McLennan S.M., Morris R.V., Graff T.G., Mertzman S.A., Ehlmann B.L., Bender S.C., Tokar R.L., Belgacem I., Newsom H., Clark B.C., Melikechi N., Mezzacappa A., McInroy R.E., Martinez R., Gasda P., Gasnault O., and Maurice S. (2016) Recalibration of the Mars Science Laboratory ChemCam instrument with an expanded geochemical database. Spectrochim. Acta, in press.

Cousin A., Meslin P.-Y., Wiens R.C., Rapin W., Mangold N., Fabre C., Gasnault O., Forni O., Tokar R., Lasue J., Vaniman D, Ollila A., Schroeder S., Sautter V., Blaney D., Le Mouelic S., Nachon M., Dromart G., Newsom H., Maurice S., Dyar M.D., Lanza N., Clark B., Clegg S., Goetz W., and the MSL Science Team (2015) Compositions of sub-millimeter-size clasts and fine particles in the Martian soils at Gale: A window into the production of soils. Icarus 249, 22-42. http://dx.doi.org/10.1016/j.icarus.2014.04/052.

Cremers D.A. and Radziemski L.J. (2006) *Handbook of Laser-Induced Breakdown Spectroscopy*, 292 pp., Wiley, San Francisco, Calif.

Crumpler L.S., Arvidson R.E., Squyres S.W., McCoy T., Yingst A., Ruff S., Farrand W., McSween H.Y., Powell M., Ming D.W., Morris R.V., Bell J.F., III, Grant J., Greeley R., DesMarais D., Schmidt M., Cabrol N.A., Haldemann A., Lewis K.W., Wang A.E., Schröder C., Blaney D., Cohen B., Yen A., Farmer J., Gellert R., Guinness E.A., Herkenhoff K.E., Johnson J.R., Klingelhöfer G., McEwen A., Rice J.W., Jr., Rice M., deSouza P., and Hurowitz J. (2011), Field reconnaissance geologic mapping of the Columbia Hills, Mars, based on Mars Exploration Rover Spirit and MRO HiRISE observations, J. Geophys. Res. 116, E00F24, doi:10.1029/2010JE003749.

Edgett K.S., Yingst R.A., Ravine M.A., Caplinger M.A., Maki J.N., Ghaemi F.T., Schaffner J.A., Bell J.F. III, Edwards L.J., Herkenhoff K.E., Heydari E., Kah L.C., Lemmon M.T., Minitti M.E., Olson T.S., Parker T.J., Rowland S.K., Schieber J., Sullivan R.J., Sumner D.Y., Thomas P.C., Jensen E.H., Simmonds J.J., Sengstacken A.J., Willson R.G., and Goetz W. (2012) Curiosity's Mars Hand Lens Imager (MAHLI) investigation. Spa. Sci. Rev. 170, 259-317. Doi:10.1007/s11214-012-9910-4.

Eigenbrode J.L., Bower H., Archer P. Jr., and the MSL Science Team (2014) Decarboxylization of carbon compounds as a potential source for CO2 and CO observed by SAM at Yellowknife Bay, Gale crater, Mars. Lunar Planet. Sci. XLV, 1605, The Lunar and Planetary Institute, Houston, TX.

Fairén A.G., Squyres S.W., Grotzinger J.P., Calvin W.M., Ruff S.W., and the MER Athena Science Team (2014) Hollowed spherules identified with the MER *Opportunity* near and at Cape York, western rim of Endeavour crater, Mars. Lunar Planet Sci. XLV, 1566, The Lunar and Planetary Institute, Houston, TX.

Forni O., Maurice S., Gasnault O., Wiens R.C., Cousin A., Clegg S.M., Sirven J.-B., and Lasue J. (2013) Independent component analysis classification of laser induced breakdown spectroscopy spectra, Spectrochim. Acta B 86, 31–41.

Forni O., Mangold N., Blaney D.L., Fisk M., Wiens R.C., Meslin P.-Y., Nachon M., Gasnault O., Maurice S., Cousin A., and Le Mouelic S. (2015) ChemCam chemostratigraphy of the Pahrump outcrop, Gale crater. Lunar Planet. Sci. XLVI, 1989, The Lunar and Planetary Institute, Houston, TX.

Freissinet C., Glavin D.P., Mahaffy P.R., Miller K.E., Eigenbrode J.L., Summons R.E., Brunner A.E., Buch A., Szopa C., Archer P.D., Franz H.B., Steele A., et al. (2014) Organic molecules in the Sheepbed mudstone, Gale Crater, Mars. Eighth International Conference on Mars, 1349, The Lunar and Planetary Institute, Houston, TX.

Freissinet, C., D. P. Glavin, P. R. Mahaffy, K. E. Miller, J. L. Eigenbrode, R. E. Summons, A. E. Brunner, A. Buch, C. Szopa, P. D. Archer, H. B. Franz, S. K. Atreya, W. B. Brinckerhoff, M. Cabane, P. Coll, P. G. Conrad, J. P. Dworkin, A. G. Fairén, P. Francois, J. P. Grotzinger, S. Kashyap, L. A. Leshin, C. A. Malespin, M. G. Martin, A. C. McAdam, D. W. Ming, R. Navarro-Gonzalez, T. Owen, A. Pavlov, B. Prats, S. W. Squyres, A. Steele, J. C. Stern, D. Y. Sumner, B. Sutter and the MSL Science Team (2015). Organic molecules in the Sheepbed Mudstone, Gale Crater, Mars. J. Geophys. Res. 120, 495–514.

Grotzinger J.P., Arvidson R.E., Bell J.F. III, Calvin W., Clark B.C., Fike D.A., Golombek M., Greeley R., Haldemann A., Herkenhoff K.E., Jolliff B.L., Knoll A.H., Malin M., McLennan S.M., Parker T., Soderblom L., Sohl-Dickstein J.N., Squyres S.W., Tosca N.J., Watters W.A. (2005) Stratigraphy and sedimentology of a dry to wet eolian depositional system, Burns Formation, Merdiani Planum, Mars. *Earth Planet. Sci. Lett. 240*, 11-72.

Grotzinger J.P., Sumner D.Y., Kah L.C., Stack K., Gupta S., Edgar L., Rubin D., Lewis K., Schieber J., Mangold N., Milliken R., Conrad P., DesMarais D., Farmer J., Siebach K., Calef F. III, Hurowitz J., McLennan S.M., Ming D., Vaniman D., Crisp J., Vasavada A., Edgett K.S., Malin M., Blake D., Gellert R., Mahaffy P., Wiens R., Maurice S., Grant J.A., Wilson S., Anderson R., Beegle L., Arvidson R., Hallet B., Sletten R., Rice M., Bell J., Griffes J., Ehlmann B., Bristow T., Palucis M., Dietrich W.E., Dromart G., Eigenbrode J., Fraeman A., Hardgrove C., Herkenhoff K., Jandura L., Kocurek G., Lee S., Leshin L.A., Leveille R., Limonadi D., Maki J., McCloskey S., Meyer M., Minitti M., Oehler D., Okon A., Newsom H., Parker T., Rowland S., Squyres S., Steele A., Stolper E., Summons R., Treiman A., Williams R., Yingst A., and the MSL Science Team (2014) A habitable fluvio-lacustrine environment at Yellowknife Bay, Gale crater, Mars. Science, 343, DOI:10.1126/science.1242777.

Grotzinger J.P., Gupta S., Rubin D.M., Schieber J., Sumner D.Y., Stack K.M., Vasavada A.R., Arvidson R.E., Calef F. III, Edgar L., Fischer W.F., Grant J.A., Kah L.C., Lamb M.P., Lewis K.W., Mangold N., Minitti M.E., Palucis M., Rice M., Siebach K., Williams R.M.E., Yingst R.A., Blake D., Blaney D., Conrad P, Crisp J., Dietrich W.E., Dromart G., Edgett K.S., Ewing R.C., Gellert R., Griffes J., Hurowitz J.A., Kocurek G., Mahaffy P., Malin M.C., McBride M.J., McLennan S.M., Mischna M., Ming D., Milliken R., Newsom H., Oehler D., Parker T.J., Vaniman D., Wiens R.C., Wilson S.A. (2015) Deposition, exhumation, and paleoclimate of an ancient lake deposit, Gale crater, Mars. *Science*, 350, aac7575, DOI: 10.1126/science.aac7575.

Gurioli L., Harris A.J.L., Colò L., Bernard J., Favalli M., Ripepe M., and Andronico D. (2013) Classification, landing distribution, and associated flight parameters for a bomb field emplaced during a single major explosion at Stromboli, Italy. *Geology 41*, 559–562.

Jacob S.R., Rowland S.K., Calef F.J. III, Stack K.M., and the MSL team (2014) Characteristics and origin of a cratered unit near the MSL Bradbury landing site (Gale crater, Mars), based on analyses of surface data and orbital imagery. Lunar Planet. Sci. XLV, 1395. The Lunar and Planetary Institute, Houston, TX.

Johnson J.R., Bell J.F. III , Bender S., Blaney D., Cloutis E., DeFlores L., Ehlmann B., Gasnault O., Gondet B., Kinch K., Lemmon M., Le Mouélic S., Maurice S., Rice M., and Wiens R.C. (2015) MSL Science Team, ChemCam Passive Reflectance Spectroscopy of Surface Materials at the Curiosity Landing Site, Mars. *Icarus* 249, 74–92, http://dx.doi.org/10.1016/j.icarus.2014.02.028.

Johnson J.R., Bell J.F. III, Bender S., Blaney D., Cloutis E., Ehlmann B., Fraeman A., Gasnault O., Kinch K., Le Mouélic S., Maurice S., Rampe E., Vaniman D., and Wiens R.C. (2016) Constraints on iron sulfate and iron oxide mineralogy from ChemCam visible/near-infrared reflectance spectroscopy of Mt. Sharp basal units, Gale Crater, Mars. *Amer. Mineralogist*, 101, 1501–1514.

Kah L., Stack K., Siebach K., Grotzinger J., Sumner D., Fairen A., Oehler D., Schieber J., Leveille R., Edgar L., Rice M., and the MSL Science Team (2014) Diagenetic features in Yellowknife Bay, Gale crater, Mars: Implications for substrate rheology and potential gas release. AAPG 2014 Annual Conference and Exhibition, April 6-9, Houston, TX. http://www.searchanddiscovery.com/abstracts/html/2014/90189ace/abstracts/1839718.html

Le Mouélic S., Gasnault O., Herkenhoff K.E., Bridges N.T., Langevin Y., Mangold N., Maurice S., Wiens R.C., Pinet P., Newsom H.E. Deen R.G., Bell J.F. III, Johnson J.R., Rapin W., Barraclough B., Blaney D.L., Deflores L., Maki J., Malin M.C., Perez R., Saccoccio M., and the MSL Science Team (2015) The ChemCam Remote Micro-Imager at Gale crater: Review of the first year of operations on Mars. Icarus, 249, 93-107; doi:10.1016/j.icarus.2014.05.030.

Loope D.B., Kettler R.M., Weber K.A., Hinrichs N.L., and Burgess D.T. (2012) Rinded iron-oxide concretions: hallmarks of altered siderite masses of both early and late diagenetic origin; Sedimentology 59, 1769–1781.

MacDonald G.A. (1972) *Volcanoes*. Prentice Hall, 544 pages.

Malin M.C., et al. (2010) The Mars Science Laboratory (MSL) mast-mounted cameras (Mastcams) flight instruments. Lunar Planet. Sci. XLI, 1123.

Mangold N., Forni O., Dromart G., Gasnault O., Nachon M., Wiens R.C., Anderson R.B., Barraclough B., Bell J.F. III, Berger G., Blaney D.L., Bridges J.C., Calef F., Clark B., Clegg S.M., Cousin A., Edgar L., Edgett K., Ehlmann B., Fabre C., Fisk M., Grotzinger J., Gupta S., Herkenhoff K.E., Hurowitz J., Johnson J.R., Kah L.C., Lanza N., Lasue J., Le Mouelic S., Leveille R., Lewin E., Malin M., McLennan S., Maurice S., Meslin P.-Y., Milliken R., Newsom H., Ollila A., Rowland S., Sautter V., Schmidt M., Schroeder S., Stack K., Summer D.Y., d'Uston C., Vaniman D., and Williams R. (2015) Chemical variations in Yellowknife Bay Formation sediments analyzed by the Curiosity rover on Mars. *J. Geophys. Res*. 120, 452-482, doi:10.1002/2014JE004681.

Marza I., Hallbauer D.K., and Forray F. (2004) Hollow, non-fixed hydrothermal concretions: A mineralogical curiosity from the Herja (Baia Mare) ore deposit. Fourth National Symposium on Economic Geology; Gold in Metaliferi Mountains, 81, 130-134.

Maurice S., Wiens R.C., Saccoccio M., Barraclough B., Gasnault O., Forni O., Mangold N., Baratoux D., Bender S., Berger G., Bernardin J., Berthé M., Bridges N., Blaney D., Bouyé M., Cais P., Clark B., Clegg S., Cousin A., Cremers D., Cros A., DeFlores L., Derycke C., Dingler B., Dromart G., Dubois B., Dupieux M., Durand E., d'Uston L., Fabre C., Faure B., Gaboriaud A., Gharsa T., Herkenhoff K., Kan E., Kirkland L., Kouach D., Lacour J.-L., Langevin Y., Lasue J., Le Mouélic S., Lescure M., Lewin E., Limonadi D., Manhes G., Mauchien P., McKay C., Meslin P.-Y., Michel Y., Miller E., Newsom H.E., Orttner G., Paillet A., Pares L., Parot Y., Perez R., Pinet P., Poitrasson F., Quertier B., Sallé B, Sotin C., Sautter V,. Seran H., Simmonds J.J., Sirven J.-B., Stiglich R., Streibig N., Thocaven J.-J., Toplis M., and Vaniman D. (2012) The ChemCam Instruments on the Mars Science Laboratory (MSL) Rover: Science Objectives and Mast Unit. Spa. Sci. Rev. 170, 95-166, DOI 10.1007/s11214-012-9912-2.

McLennan S.M., Anderson R.B., Bell J.F. III, Bridges J.C., Calef F. III, Campbell J.L., Clark B.C., Clegg S., Conrad P., Des Marais D.J., Dromart G., Dyar M.D., Edgar L.A., Ehlmann B.L.,

Fabre C., Forni O., Gasnault O., Gellert R., Gordon S., Grant J.A., Grotzinger J.P. Gupta S., Herkenhoff K.E., Hurowitz J.A., King P.L., Le Mouelic S., Leshin L.A., Leveillé R., Lewis K.W., Mangold N., Maurice S., Ming D., Morris R.V., Nachon M., Newsom H.E., Ollila A.M., Perret G.M., Rice M.S., Schmidt M.E., Schwenzer S.P., Stack K., Stolper E.M., Sumner D.Y., Treiman A.H., van Bommel S., Vaniman D.T., Vasavada A., Wiens R.C., and Yingst R.A. (2014) Elemental geochemistry of sedimentary rocks in Yellowknife Bay, Gale Crater, Mars. *Science 343 DOI: 10.1126/science.1244734*.

Ming D.W., Archer P.D., Jr., Glavin D.P., Eigenbrode J.L, Franz H.B., Sutter B., Brunner A.E., Stern J.C., Freissinet C., McAdam A.C., Mahaffy P.R., Cabane M., Coll P., Campbell J.L., Atreya S.K., Niles P.B., Bell J.F. III, Bish D.L., Brinckerhoff W.B., Buch A., Conrad P.G., Des Marais D.J., Ehlmann B.L., Fairen A.G., Farley K., Flesch G.J., Francois P., Gellert R., Grant J.A., Grotzinger J.P., Gupta S., Herkenhoff K.E., Hurowitz J.A., Leshin L.A., Lewis K.W., McLennan S.M., Perrett G.M., Pradler I., Squyres S.W., Summons R.E., Steele A., Stolper E.M., Sumner D.Y., Szopa C., Teinturier S., Trainer M.G., Treiman A.H., Vaniman D.T., Vasavada A.R., Webster C.R., Wray J.J., Yingst R.A., and the MSL Science Team (2014) Volatile and organic compositions of sedimentary rocks in Yellowknife Bay, Gale crater, Mars. *Science* 343, doi: 10.1126/science.1245267.

Misra A.K., Acosta-Maeda T.E., Scott E.R.D., and Sharma S.K. (2014) Possible mechanism for explaining the origin and size distribution of Martian hematite spherules. *Planet. Spa. Sci*. 92, 16-23.

Morris R.V., Ruff S.W., Gellert R., Ming D.W., Arvidson R.E., Clark B.C., Golden D.C., Siebach K., Klingelhoefer G., Schroeder C., Fleischer I., Yen A.S., and Squyres S.W. (2010) Identification of carbonate-rich outcrops on Mars by the Spirit rover. *Science* 329, 421-424, doi:10.1126/science.1189667.

Nachon M., Clegg S.M., Mangold N., Schroeder S., Kah L.C., Dromart G., Ollila A., Johnson J., Oehler D., Bridges J., Le Mouelic S., Wiens R.C., Anderson R., Blaney D., Bell J.F., Clark B., Cousin A., Dyar M.D., Ehlmann B., Fabre C., Forni O., Gasnault O., Grotzinger J., Lasue J., Lewin E., Leveillé R., McLennan S., Maurice S., Meslin P.-Y., Rice M., Stack K., Vaniman D., Wellington D., and the MSL Science Team (2014) Calcium sulfate veins characterized by the ChemCam instrument at Gale crater, Mars. *J. Geophys. Res.*, 119, 1991-2016, doi:10.1002/2013JE004588.

Oze C. and Sharma M. (2005) Have olivine, will gas: Serpentinization and the abiogenic production of methane on Mars, *Geophys. Res. Lett*. 32, L10203, DOI: 10.1029/2005GL022691.

Palucis M.C., Dietrich W.E., Hayes A.G., Williams R.M.E., Gupta S., Mangold N., Newsom H., Hardgrove C., Calef F. III, and Sumner D.Y. (2014) The origin and evolution of the Peace Vallis fan system that drains to the *Curiosity* landing area, Gale crater, Mars. *J. Geophys. Res. Planets* 119, 705-728, doi:10.1002/2013JE004583.

Palucis M.C., Dietrich W.E., Williams R.M.E., Hayes A.G., Parker T., Sumner D.Y., Mangold N., Lewis K., and Newsom H. (2016) Sequence and relative timing of large lakes in Gale crater (Mars) after the formation of Mount Sharp. *J. Geophys. Res. Planets* 121, doi:10.1002/2015JE004905.

Payré V., C. Fabre, A. Cousin, O. Forni, O. Gasnault, W. Rapin, W. Goetz, M. Nachon, V. Sautter, L. Le Deit, S. Maurice, R.C. Wiens, S. Clegg (2016a) Trace elements in Gale crater: Li, Sr, Rb, and Ba abundances using ChemCam data. Lunar Planet Sci. XLVII, 1348, The Lunar and Planetary Institute, Houston, TX.

Payré V., C. Fabre, A. Cousin, O. Forni, O. Gasnault, W. Rapin, W. Goetz, M. Nachon, V. Sautter, L. Le Deit, S. Maurice, R.C. Wiens, S. Clegg (2016b) Copper abundances in Gale crater: First ChemCam calibration and quantification. Lunar Planet Sci. XLVII, 1347, The Lunar and Planetary Institute, Houston, TX.

Potter S.L. and Chan M.A. (2011) Joint controlled fluid flow patterns and iron mass transfer in Jurassic Navajo Sandstone, Southern Utah, USA. *Geofluids* 11, 184-198, doi: 10.1111/j.1468-8123.2011.00329.x.

Potter S.L., Chan M.A., Peterson E.U., Dyar M.D., and Sklute E. (2011) Characterization of Navajo Sandstone concretions: Mars comparison and criteria for distinguishing diagenetic origins. *Earth Planet. Sci. Lett*. 301, 444-456.

Putthapiban P. and Hongsresawat S. (2007) Formation of hollow concretions in northeastern *Thailand. Adv. Geosci*. 13, 13-22.

Raiswell R. (1971) The growth of Cambrian and Liassic concretions. *Sedimentology* 17, 147-171.

Rubin D.M., Fairen A., Frydenvang J., Gasnault O., Gelfenbaum G., Goetz W., Grotzinger J.P., LeMouelic S., Mangold N., Newsom H., Oehler D.Z., Rapin W., and Wiens R.C. (2016) Fluidized sediment pipes in Gale crater, Mars, and possible analogs in the Middle Jurassic of Utah. *Geology*, 45, 7-10, doi:10.1130/G38339.1.

Schmid R. (1981) Descriptive nomenclature and classification of pyroclastic deposits and fragments: Recommendations of the lUGS Subcommission on the Systematics of Igneous Rocks. *Geology* 9, 41-43.

Schroeder S., Meslin P.-Y., Gasnault O., Maurice S., Cousin A., Forni O., Mangold N., Rapin W., Le Mouelic S., Ollila A., Nachon M., Lasue J., Dyar M.D., Clegg S., Jackson R., and Wiens R.C. (2015) First analysis of the hydrogen signal in ChemCam LIBS spectra. *Icarus*, 249, 43-61; doi.org/10.1016/j.icarus.2014.08.029.

Schwenzer S.P., Abramov O., Allen C.C., Bridges J.C., Clifford S.M., Filiberto J., Kring D.A., Lasue J., McGovern P.J., Newsom H.E., Treiman A.H., Vaniman D.T., Wiens R.C., and Wittmann A. (2012) Gale crater: Formation and post-impact hydrous environments. *Planet. Spa. Sci*. 70, 84-95.

Simpson E., Betts T.A., Sherrod L.A., Wizevich M.C., Morgano K., Richardson A., Malenda M., Simpson W.S., Livingston K., and Bogner E. (2016) Voids: Small-scale, gas-generated soft sediment deformation structures found in deltaic muds of the Lake Powell delta, Glen Canyon National Recreation Area, Hite, Utah. Geological Soc. Am. Meeting, paper 82-4, https://gsa.confex.com/gsa/2016AM/webprogram/Paper280538.html.

Smith W.E. (1957) Pyrite nodules in the Hythe Beds of the Tilburstow Hill area, Surrey. Proc. Geol. Assoc. 68, 45-52.

Squyres S.W., Grotzinger J.P., Arvidson R.E., Bell J.F. III, Calvin W., Christensen P.R., Clark B.C., Crisp J.A., Farrand W.H., Herkenhoff K.E., Johnson J.R., Klingelhoefer G., Knoll A.H., McLennan S.M., McSween H.Y., Morris R.V., Rice J.W., Rieder R., Soderblom L.A. (2004) In situ evidence for an ancient aqueous environment at Meridiani Planum, Mars. *Science 306*, 1709-1714.

Stack K.M., Grotzinger J.P., Kah L.C., Schmidt M.E., Mangold N., Edgett K.S., Siebach K.L., Nachon M., Lee R., Blaney D.L., Deflores L.P., Edgar L.A., Fairen A.G., Leshin L.A., Maurice S., Oehler D.Z., Rice M.S., Sumner D.Y., and Wiens R.C. (2014) Diagenetic origin of nodules and hollow nodules of the Sheepbed Member, Yellowknife Bay Formation, Gale crater, Mars. *J. Geophys. Res*. 119, 1637-1664, doi:10.1002/2014JE004617.

Stack K.M., Edwards C.S., Grotzinger J.P., Gupta S., Sumner D.Y., Calef F.J. III, Edgar L.A., Edgett K.S., Fraeman A.A., Jacob S.R., Le Deit L., Lewis K.W., Rice M.S., Rubin D., Williams R.M.E., and Williford K.H. (2016) Comparing orbiter and rover image-based mapping of an ancient sedimentary environment, Aeolis Palus, Gale crater, Mars. *Icarus* 280, 3-21, doi:10.1016/j.icarus.2016.02.024.

Stauffer M.R. and Butler S.L. (2010) The Shapes of Splash-Form Tektites: Their Geometrical Analysis, Classification and Mechanics of Formation; *Earth Moon Planets* 107, 169–196, DOI 10.1007/s11038-010-9359-y.

Stöffler D. and Grieve R. A. F. (2007) Impactites, Chapter 2.11 in Fettes, D. and Desmons, J. (eds.) Metamorphic Rocks: A Classification and Glossary of Terms, Recommendations of the International Union of Geological Sciences, Cambridge University Press, Cambridge, UK, 82-92, 111-125, and 126-242.

Treiman A.H., Bish D.L., Vaniman D.T., Chipera S.J., Blake D.F., Ming D.W., Morris R.V., Bristow T.F., Morrison S.M., Baker M.B., Rampe E.B., Downs R.T., Filiberto J., Glazner A.F., Gellert R., Thompson L.M., Schmidt M.E., Le Deit L., Wiens R.C., McAdam A.C., Achilles C.N., Edgett K.S., Farmer J.D., Fendrich K.V., Grotzinger J.P., Gupta S., Morookian J.M., Newcombe M.E., Rice M.S., Spray J.G., Stolper E.M., Sumner D.Y., Vasavada A.R., and Yen A.S. (2016) Mineralogy, provenance, and diagenesis of a potassic basaltic sandstone on Mars: CheMin x0ray diffraction of the Windjana sample (Kimberley area, Gale Crater). *J. Geophys. Res. Planets* 121, 75-106, doi:10.1002/2015JE004932.

Van der Burg W.J. (1969) The formation of rattle stones and the climatological factors which limited their distribution in the Dutch Pleistocene, 1: The formation of rattle stones. *Paleogeography, Paleoclimatology, Paleoecology*, 6, 105-124.

Vaniman D.T., Bish D.L., Ming D.W., Bristow T.F., Morris R.V., Blake D.F., Chipera S.J., Morrison S.M., Treiman A.H., Rampe E.B., Rice M., Achilles C.N., Grotzinger J., McLennan S.M., Williams J., Bell J. III, Newsom H., Downs R.T., Maurice S., Sarrazin P., Yen A.S., Morookian J.M., Farmer J.D., Stack K., Milliken R.E., Ehlmann B., Sumner D.Y., Berger G., Crisp J.A., Hurowitz J.A., Anderson R., DesMarais D., Stolper E.M., Edgett K.S., Gupta S., Spanovich N., and the MSL Science Team (2014) *Science*, 343, DOI: 10.1126/science.1243480.

Webster C.R., Mahaffy P.R., Atreya S.K., Flesch G.J., Mischna M.A., Meslin P.-Y., Farley K.A., Conrad P.G., Christensen L.E., Pavlov A.A., Martin-Torres J., Zorzano M.-P., McConnochie T.H., Owen T., Eigenbrode J.L., Glavin D.P., Steele A., Malespin C.A., Archer P.D. Jr., Sutter B., Coll P., Freissinet C., McKay C.P., Moores J.E., Schwenzer S.P., Bridges J.C., Navarro-Gonzalez R., Gellert R., Lemmon M.T., and the MSL Science Team (2014) Mars methane detection and variability at Gale crater. *Science* 343, 10.1126/science.1261713.

Wiens R.C., Maurice S., Barraclough B., Saccoccio M., Barkley W.C, Bell J.F. III, Bender S., Bernardin J., Blaney D., Blank J., Bouye M., Bridges N., Cais P., Clanton R.C., Clark B., Clegg S., Cousin A., Cremers D., Cros A., DeFlores L., Delapp D., Dingler R., D'Uston C., Dyar M.D., Elliott T., Enemark D., Fabre C., Flores M., Forni O., Gasnault O., Hale T., Hays C., Herkenhoff K., Kan E., Kirkland L, Kouach D., Landis D., Langevin Y., Lanza N., LaRocca F., Lasue J., Latino J., Limonadi D., Lindensmith C., Little C., Mangold N., Manhes G., Mauchien P., McKay C., Miller E., Mooney J., Morris R.V., Morrison L., Nelson T., Newsom H., Ollila A., Ott M., Pares L., Perez R., Poitrasson F., Provost C., Reiter J.W., Roberts T., Romero F., Sautter V., Salazar S., Simmonds J.J., Stiglich R., Storms S., Streibig N., Thocaven J.-J., Trujillo T., Ulibarri M., Vaniman D., Warner N., Waterbury R., Whitaker R., Witt J., and Wong-Swanson B. (2012) The ChemCam Instruments on the Mars Science Laboratory (MSL) Rover: Body Unit and Combined System Performance. *Spa. Sci. Rev.* 170, 167-227, doi 10.1007/S11214-012-9902-4.

Wiens R.C., Maurice S., Lasue J., Forni O., Anderson R.B., Clegg S., Bender S., Barraclough B.L., Deflores L., Blaney D., Perez R., Lanza N., Ollila A., Cousin A., Gasnault O., Vaniman D., Dyar M.D., Fabre C., Sautter V., Delapp D., Newsom H., Melikechi N., and the ChemCam team (2013) Pre-flight calibration and initial data processing for the ChemCam laser-induced breakdown spectroscopy instrument on the Mars Science Laboratory rover. *Spectrochim. Acta* B, 82, 1-27, http://dx.doi.org/10.1016/j.sab.2013.02.003.

Wiens R.C., Maurice S., Gasnault O., Clegg S., Fabre C., Nachon M., Rubin D., Goetz W., Mangold N., Schroeder S., Rapin W., Milliken R., Fairen A.G., Oehler D., Forni O., Sautter V., Blaney D., Le Mouelic S., Anderson R.B., Cousin A., Vasavada A., and Grotzinger. J.P. (2015) Centimeter to decimeter size spherical and cylindrical features in Gale crater sediments. Lunar Planet. Sci. XLVI, 1249, The Lunar and Planetary Institute, Houston, TX.

Williams R.M.E., Grotzinger J.P., Dietrich W.E., Gupta S., Sumner D.Y., Wiens R.C., Mangold N., Malin M.C., Edgett K.S., Maurice S., Forni O., Gasnault O., Ollila A., Newsom H.E., Dromart G., Palucis M.C., Yingst R.A., Anderson R.B., Herkenhoff K.E., Le Mouelic S., Goetz W., Madsen M.B., Koefoed A., Jensen J.K., Bridges J.C,. Schwenzer S.P., Lewis K.W., Stack K.M., Rubin D., Kah L.C., Bell J.F., Farmer J.D., Sullivan R., Van Beek T., Blaney D.L., Pariser O., Deen R.G., and the MSL Science Team. (2013) Martian fluvial conglomerates at Gale Crater. *Science* 340, 1068-1072, DOI: 10.1126/science.1237317

Williams R.M.E., Malin M.C., Edgar L. Lewis K.S. (2016) Bedding geometry of bench-forming strata in the Kylie and Kimberley regions of Gale Crater, GSA Abstracts with Programs, vol. 47, no. 7, Abstract #266584.

Young, R.W., Wray, R.A.L. &. Young, A.R.M. (2009) *Sandstone landforms*, Cambridge University Press, Cambridge.

Table 1. Major-element relative abundances in wt. % for individual observation points of the Winnipesaukee target.

Point	SiO_2	TiO_2	Al_2O_3	FeO_T	MgO	CaO	Na_2O	K_2O	Total[1]
1	64.3	0.68	17.5	4.1	1.7	4.5	4.86	3.57	101.1
2	54.4	0.72	22.6	1.4	0.6	10.4	6.65	1.00	97.9
3	62.3	0.66	14.2	7.4	2.7	8.0	5.38	3.29	104.0
4	48.6	0.89	15.8	16.0	5.0	8.9	2.94	0.64	98.8
5	40.7	0.91	8.9	18.3	7.5	7.6	1.98	0.27	86.2
6	54.7	0.76	19.9	13.9	2.0	0.9	4.68	3.66	100.5
7	46.7	1.27	11.5	20.2	3.8	4.6	3.56	2.14	93.7
8	48.3	0.74	7.2	15.7	4.9	12.0	3.54	0.61	93.0
9	64.5	0.32	20.8	0.4	0.5	1.9	5.81	3.17	97.4
10	59.8	0.76	17.8	7.4	1.6	2.6	4.48	3.56	97.9
Precision[2]	*0.4*	*0.05*	*0.1*	*0.3*	*0.1*	*0.3*	*0.11*	*0.04*	

[1]Excluding SO_3, CO_2, H_2O, Cl; see text for description.

[2]Within the raster; Blaney et al. (2015)

Table 2. Major-element abundances (wt. %) and qualitative hydration of the Winnipesaukee spheroidal object and host rock.

		SiO_2	TiO_2	Al_2O_3	FeO_T	MgO	CaO	Na_2O	K_2O	Hydration
Host Rock (points 1, 9, 10)	Mean	62.9	0.59	18.7	4.0	1.3	3.0	5.05	3.43	Moderate
	Std dev	*2.7*	*0.23*	*1.8*	*3.5*	*0.7*	*1.3*	*0.69*	*0.23*	
Spheroid Exterior (points 6-8)	Mean	49.9	0.92	12.9	16.6	3.6	5.8	3.93	2.14	Moderate
	Std dev	*4.2*	*0.30*	*6.5*	*3.2*	*1.5*	*5.7*	*0.65*	*1.52*	
Soil, points 4 & 5, first 10 shots		43.2	1.00	9.7	18.5	7.0	7.5	2.12	0.40	Higher
Interior, point 4, last 10 shots		50.7	0.84	17.4	13.8	4.1	8.9	3.60	0.75	Higher

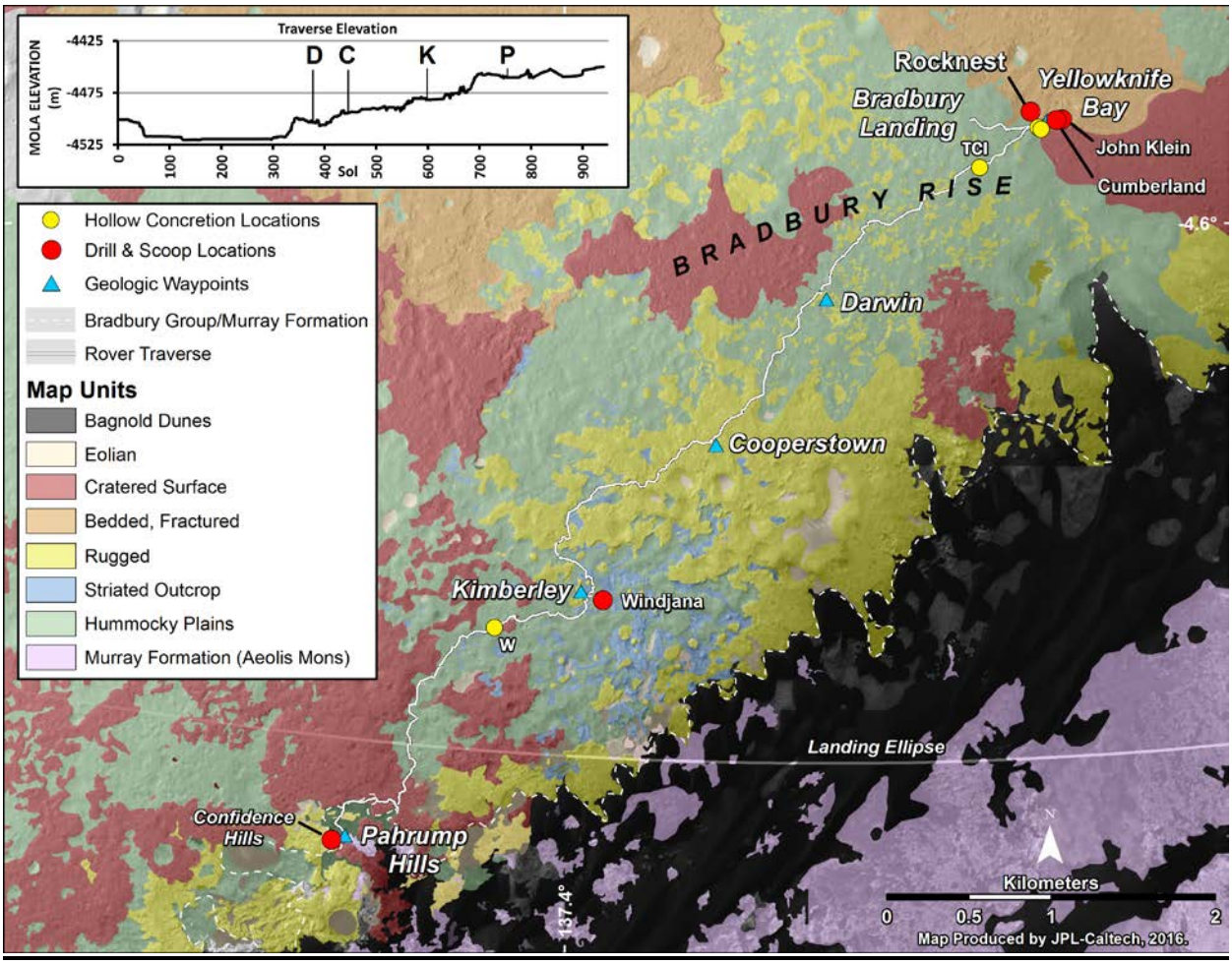

Fig. 1. Rover traverse map in Gale crater up to sol 800. An inset shows the elevations of the waypoints indicated on the map. Yellow circles indicate the locations of the features discussed in this work. Twin Cairns Island ("TCI") is just southwest of Yellowknife Bay on Bradbury Rise. The target Winnipesaukee ("W") is just west of the Kimberley outcrop, still well within the landing ellipse, and approximately 6 km from the Yellowknife Bay area. Tochatwi and Point Lake, indicated by unmarked yellow circles, are shown in greater detail in Fig. 2.

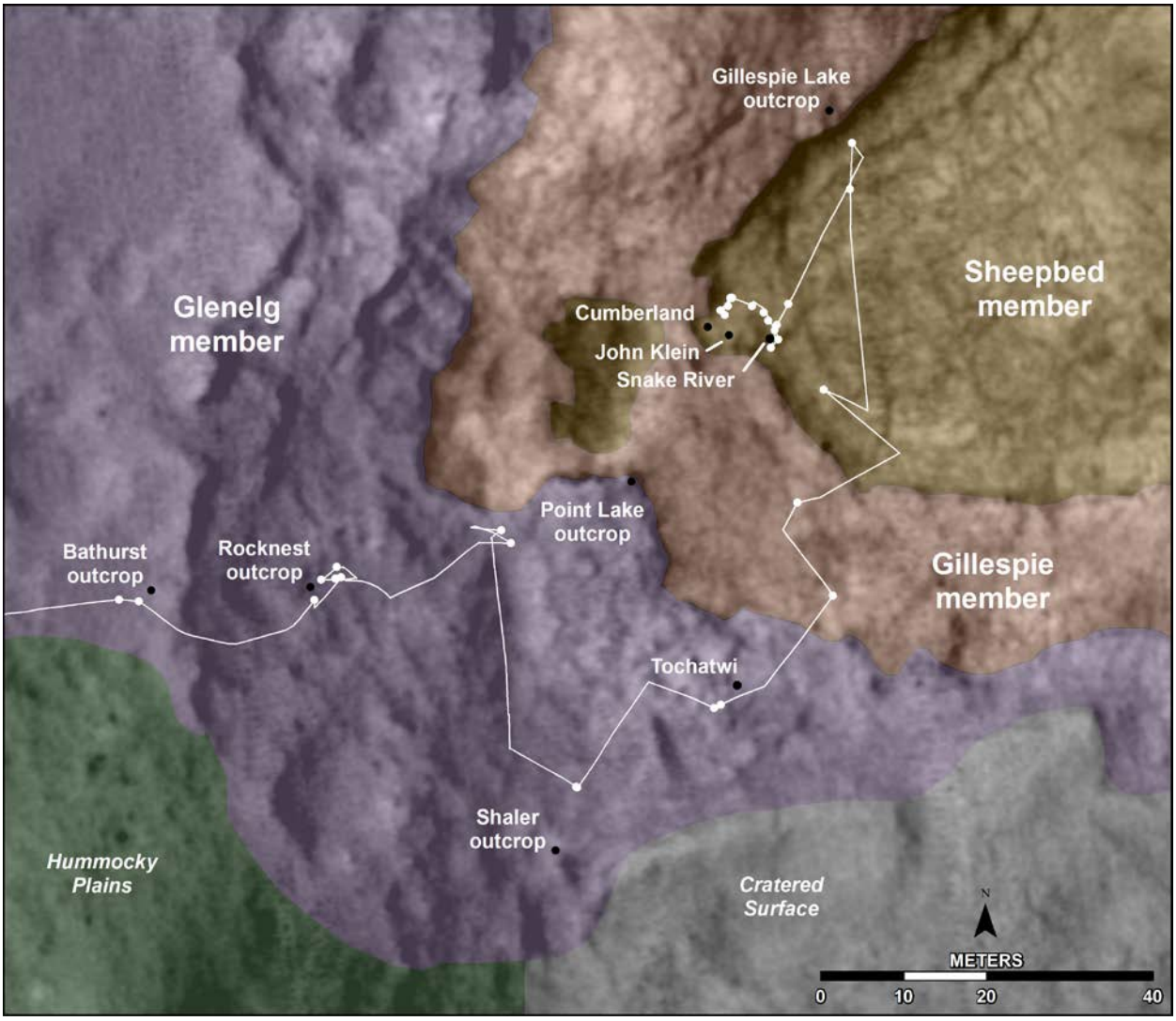

Fig. 2. Overhead view of the Yellowknife Bay (YKB) area with identification of the different members, after Grotzinger et al. (2014). The rover traverse into YKB is indicated by the white line with stopping locations as white points. Dark points indicate targeted outcrops, objects of interest, and drill holes. After sampling Sheepbed the rover visited Point Lake and revisited Shaler before driving away.

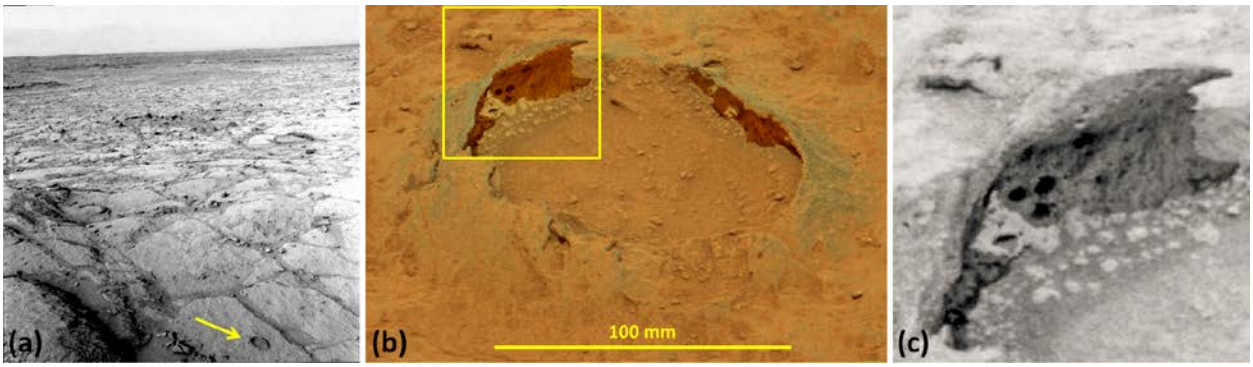

Fig. 3. Images of Tochatwi, an apparent thin-walled spheroidal feature observed protruding from the Glenelg member sandstone on sol 122. (a) Navcam context image with arrow indicating the feature. (b) Mastcam image of Tochatwi. Image portions of the shadowed areas have been modified slightly (brightness and contrast were adjusted) for better visibility. Panel (c), enlarged view of the interior wall of Tochatwi.

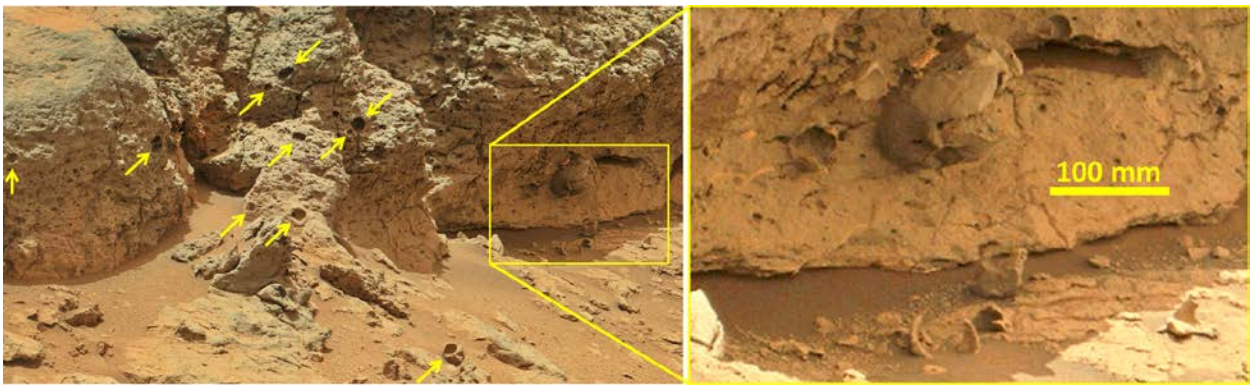

Fig. 4. Point Lake outcrop showing 3 cm size voids (yellow arrows). Inset shows a ~10 cm diameter spheroidal object along with portions of several hollow spheroidal shells. The view seen in the inset was taken from a slightly different angle.

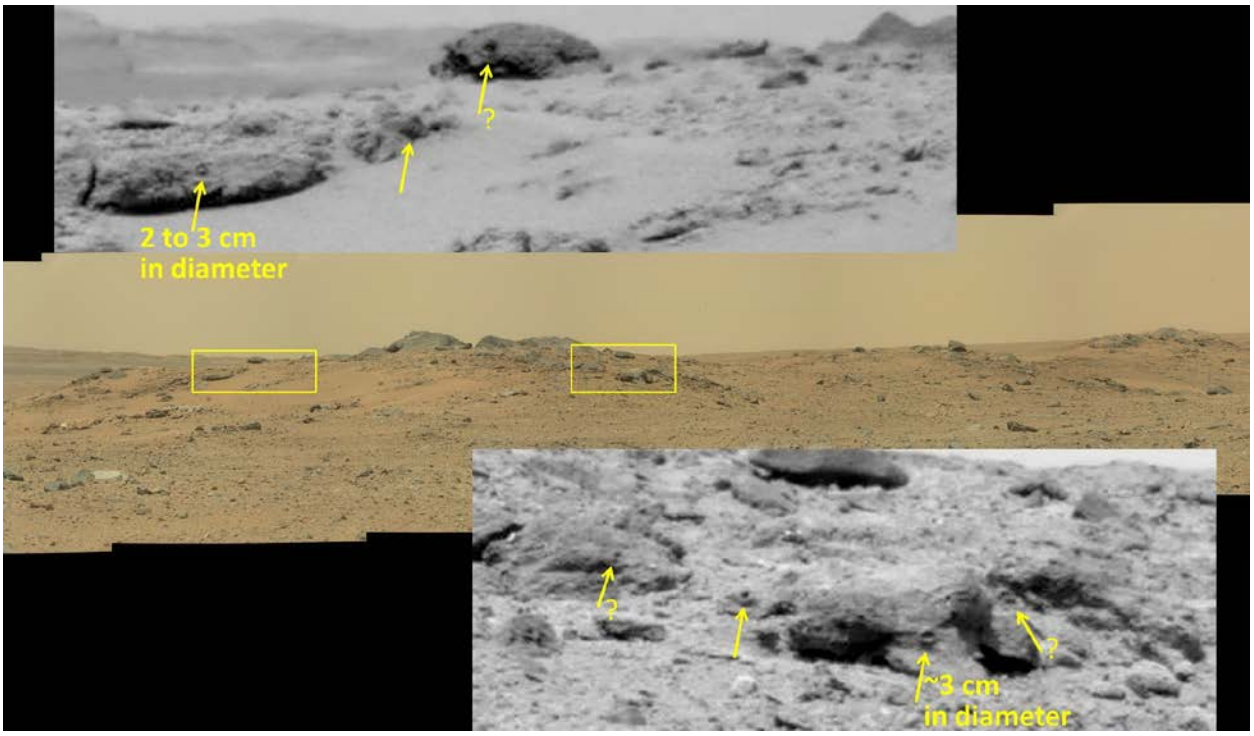

Fig. 5. Mastcam mosaic of Twin Cairns Island. Insets with arrows show apparent voids 2.5-3 cm in diameter in the outcrop that appear similar to those at Point Lake.

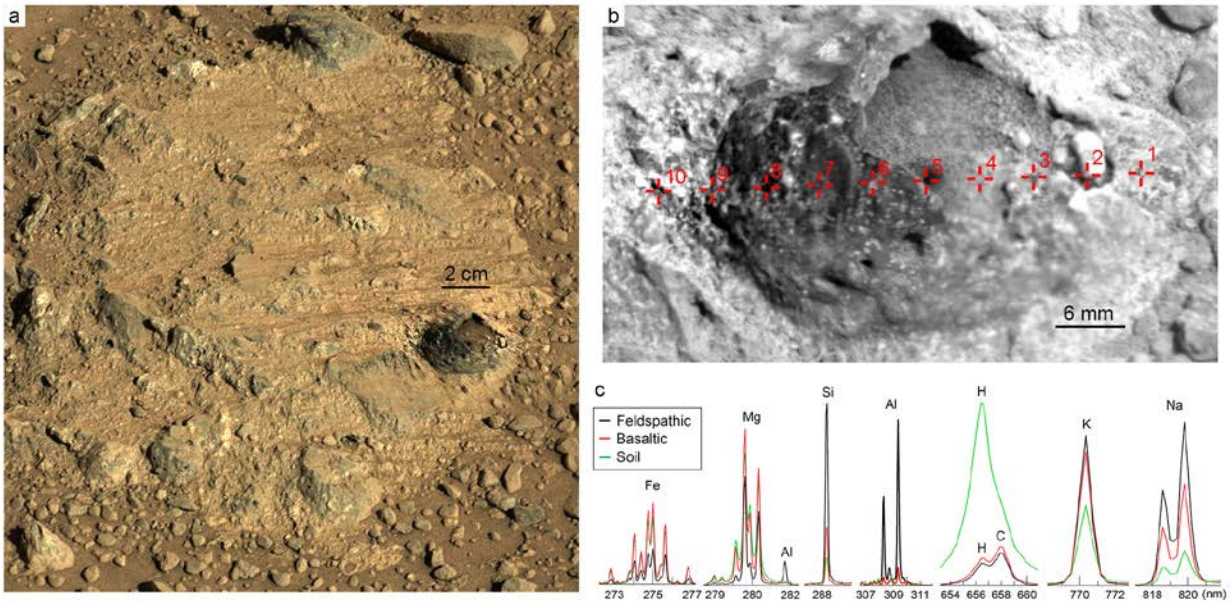

Fig. 6. Winnipesaukee spheroidal feature. (a) Mastcam view of feature within its light-toned host rock. In addition to the Winnipesaukee feature, several other dark-toned clasts are present embedded in the host rock. Some to the lower left portion of the image contain vugs. (b) RMI image with LIBS locations indicated in red. The images for the mosaic were taken during the course of the LIBS raster. The image used for the right side was taken before point 4 while the image used for the right side was taken after point 5, which left a divot in the soil in the center of the sphere. (c) Selected LIBS spectral regions showing significant differences between the host rock (points 1, 9, 10, indicated as Feldspathic), exterior of the sphere (point 6-8, Basaltic), and soil inside the sphere (points 4, 5, Soil).

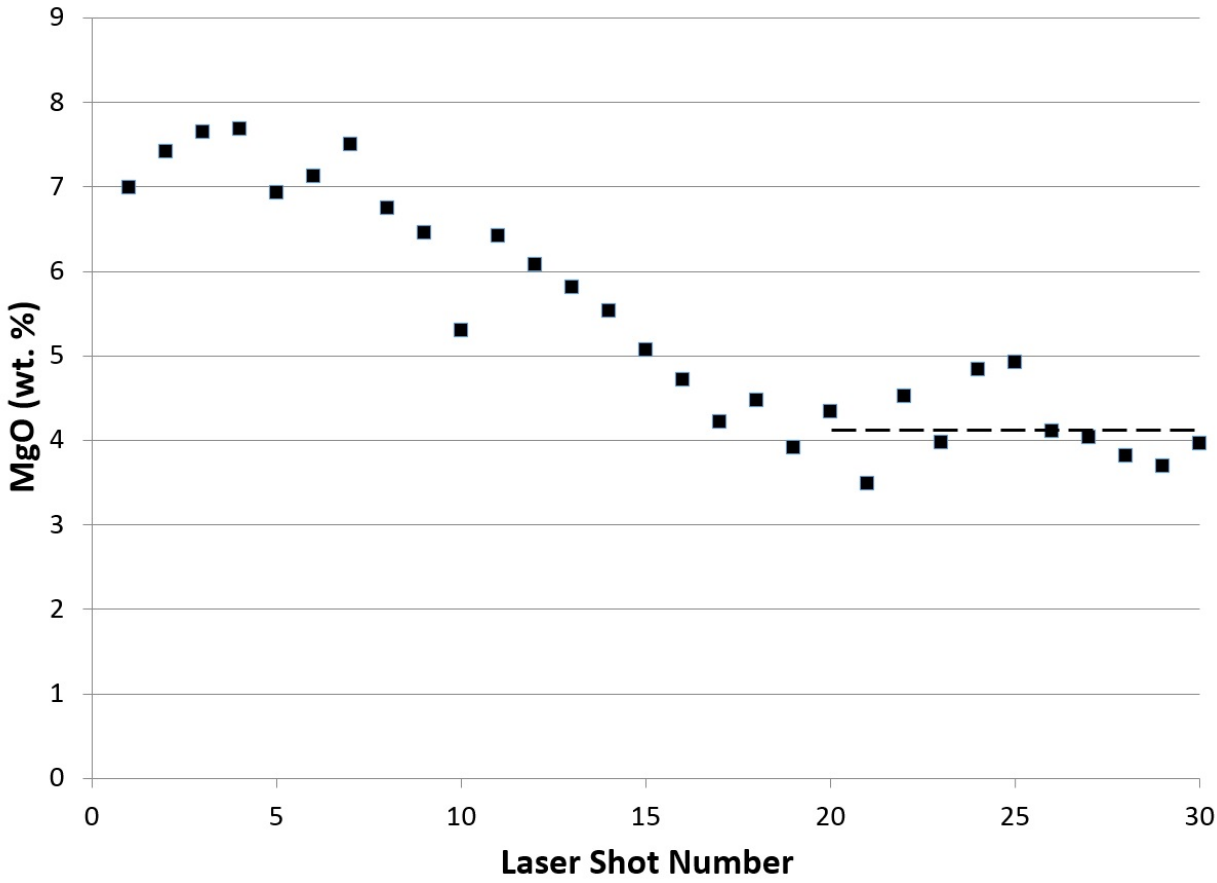

Fig. 7. Depth profile of MgO abundances from Winnipesaukee observation point 4. The initial composition is consistent with soil accumulated inside the spheroidal shell. The composition changes starting around shot 9, indicating a different and solid material was probed with the last shots. The dashed line indicates the mean composition of the last ten shots.

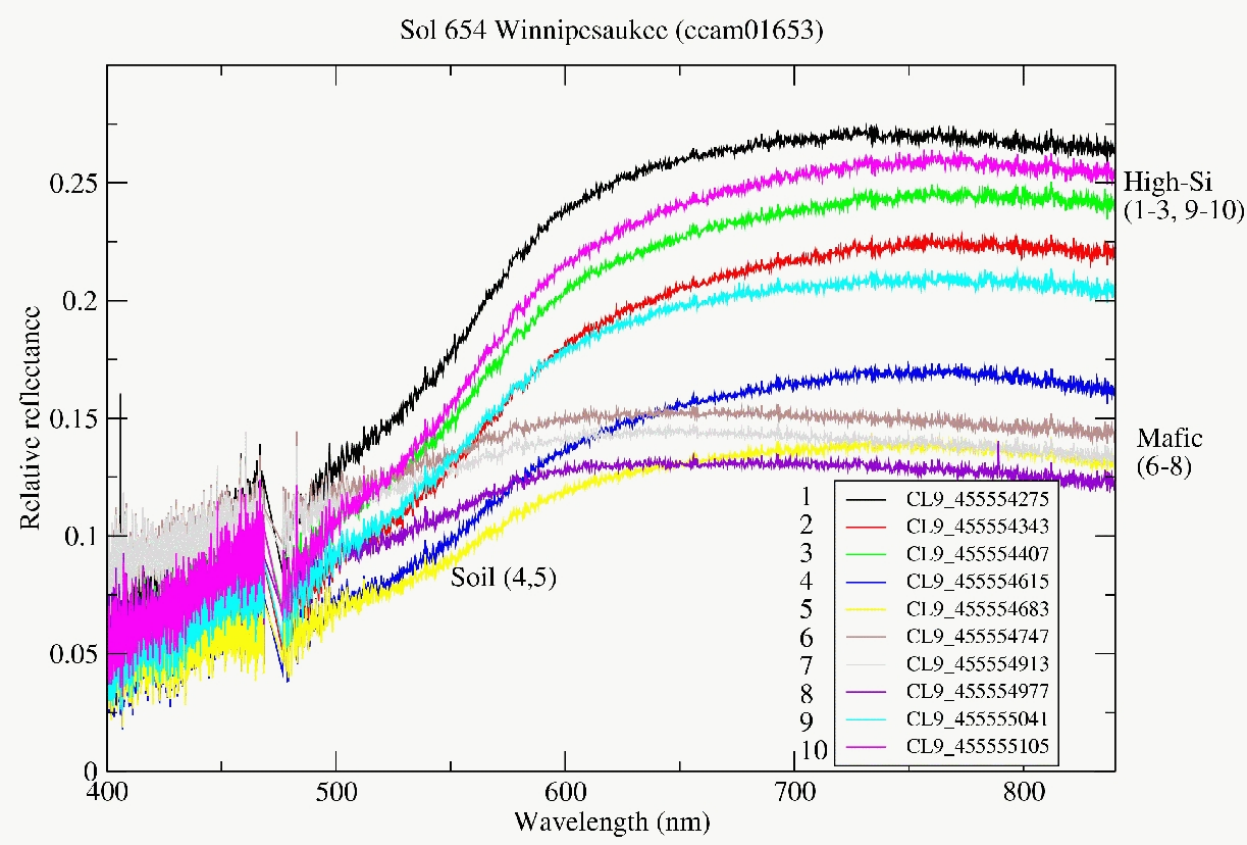

Fig. 8. Passive reflectance spectra taken by ChemCam without the laser. Observation points 1-10, corresponding to the positions indicated in Fig. 6, are represented by different color spectra.

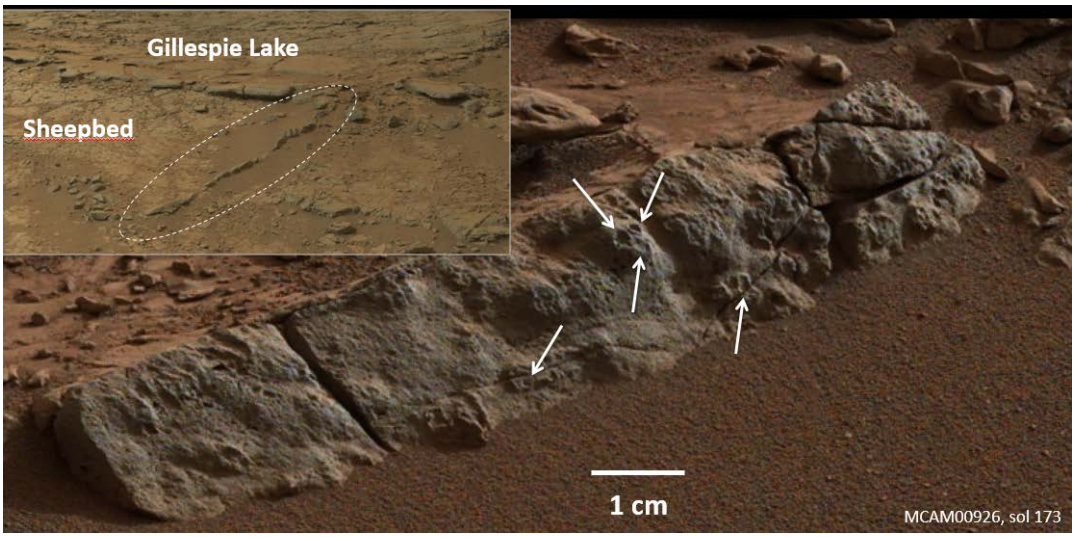

Fig. 9. The snake (inset, arrows), an apparent sedimentary dike feature, < 10 m from the Cumberland drill hole. Gillespie Lake and Sheepbed members are indicated in the inset. Arrows in the close-up image show voids in the dike material.

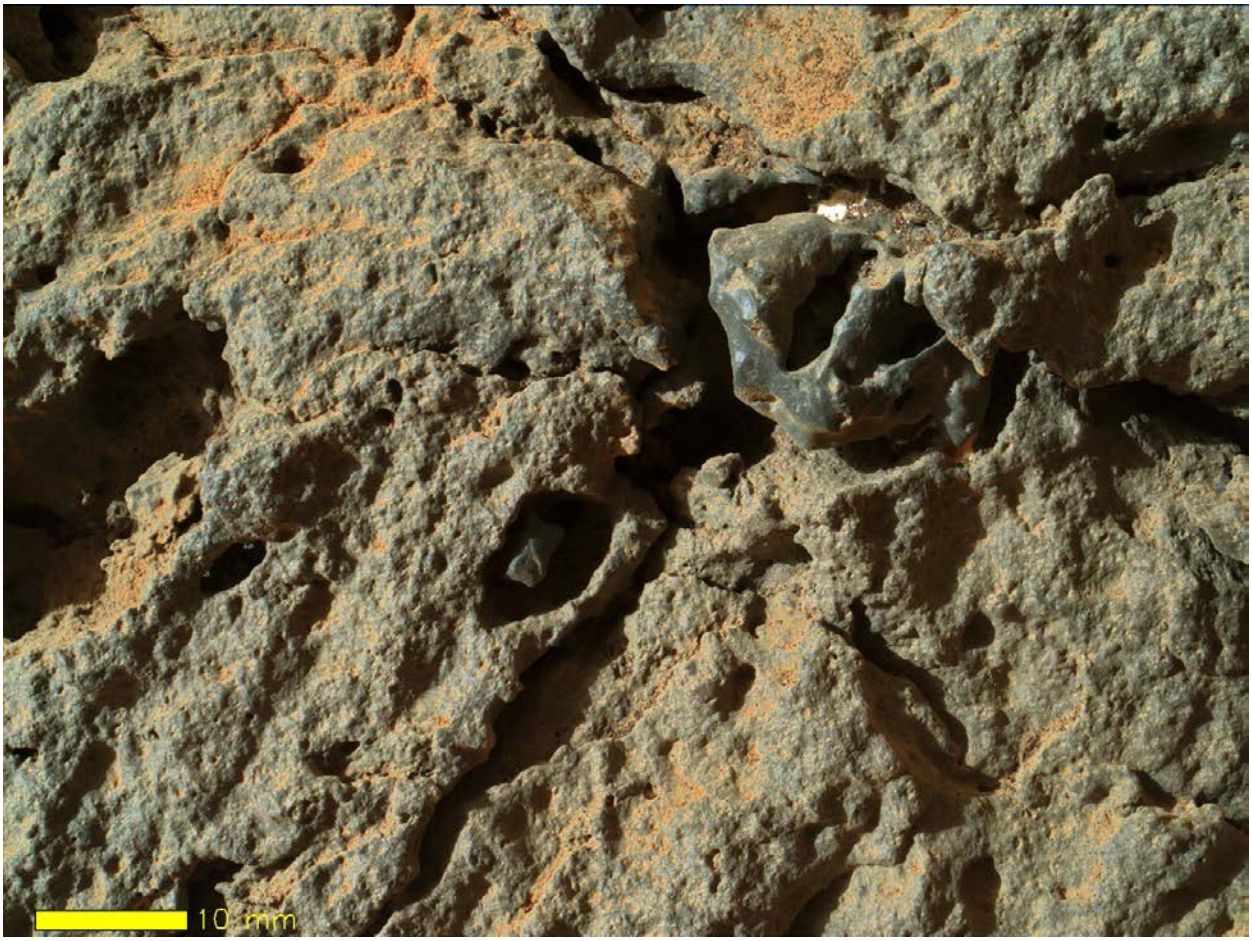

Fig. 10. Point Lake voids with remnant material inside.

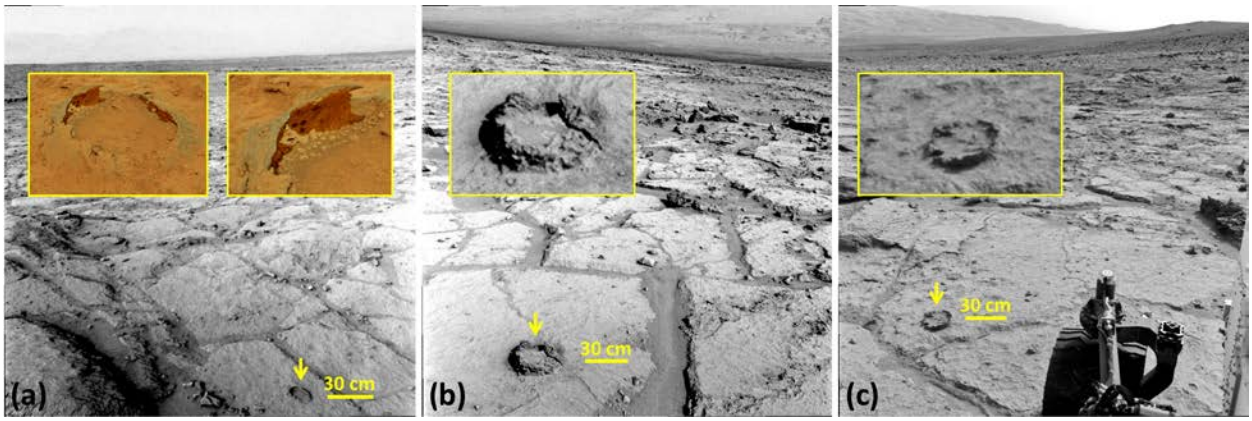

Fig. S1 Images of Tochatwi as well as two potentially related features in the area.

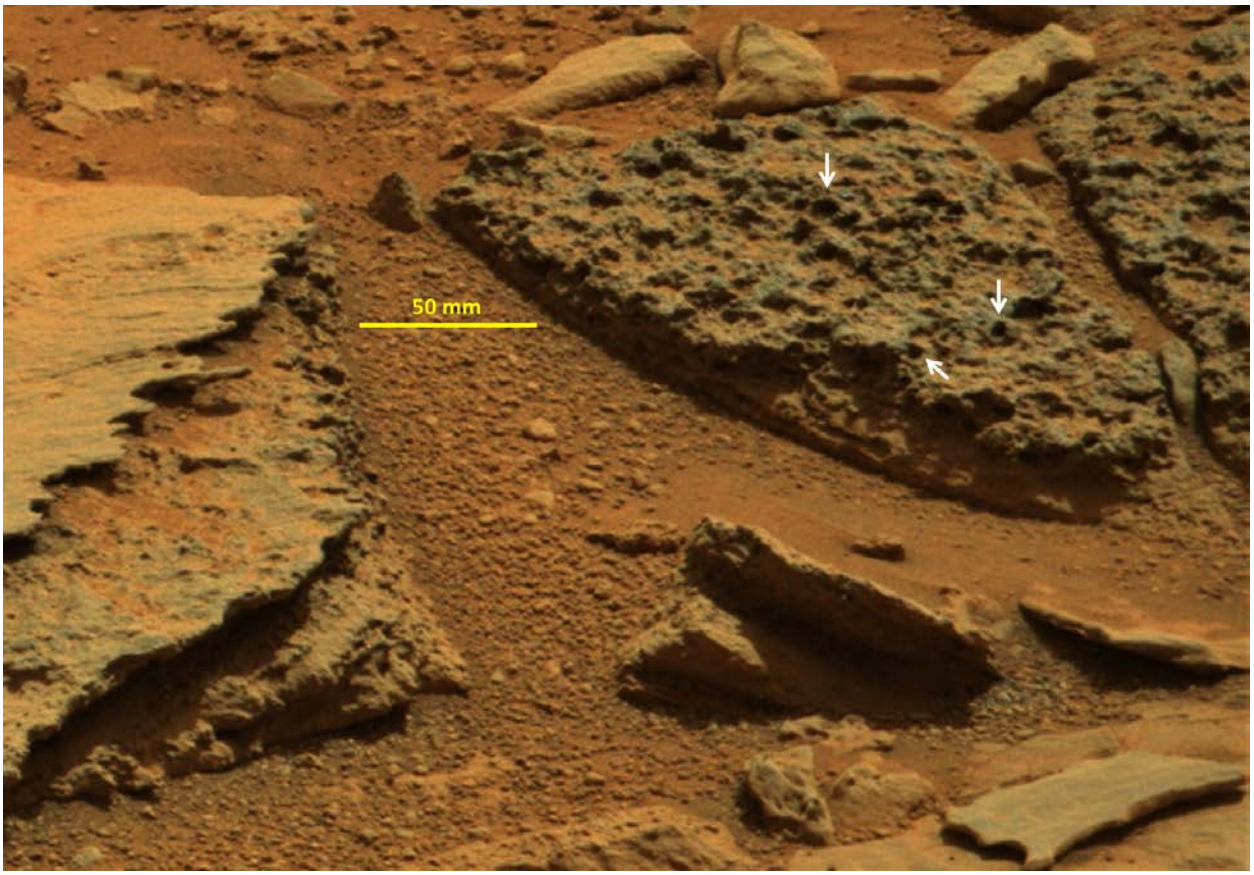

Fig. S2. Mastcam image of a pitted layer near the Shaler outcrop, imaged on sol 121. Arrows point to conspicuous spheroidal voids.

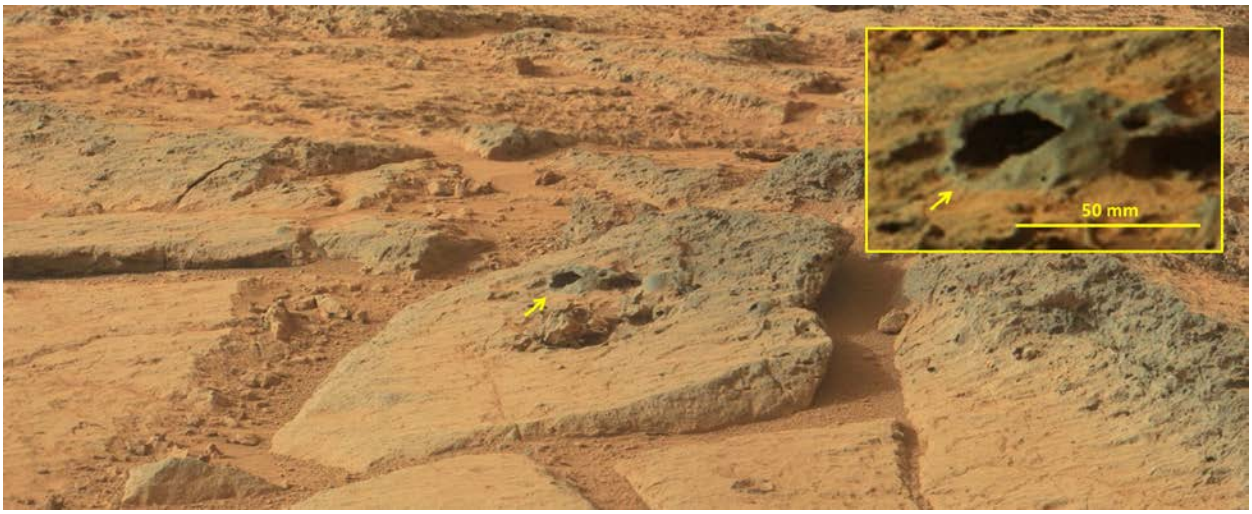

Fig S3. Hollow spheroid similar to Winnipesaukee, observed near Shaler on sol 306.

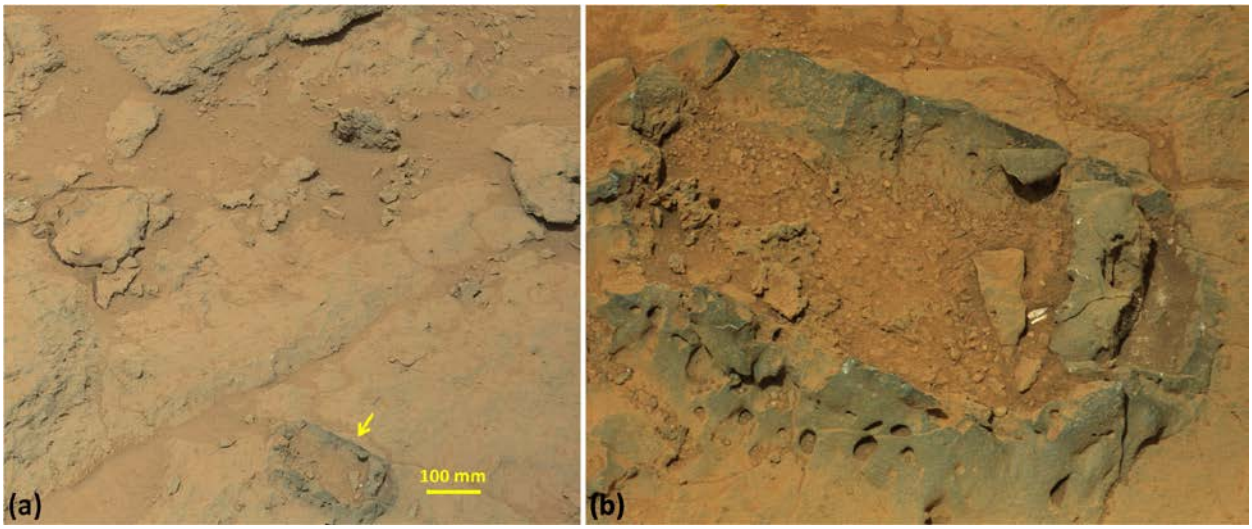

Fig. S4. Object observed on sol 308 near Shaler. It may be related to either the hollow spheroids or to sedimentary pipes. Note the vesicular morphology in the walls.

Fig. S5. Transitional features between voids and hollow spheroids, from the Kimberley outcrop, sol 597.

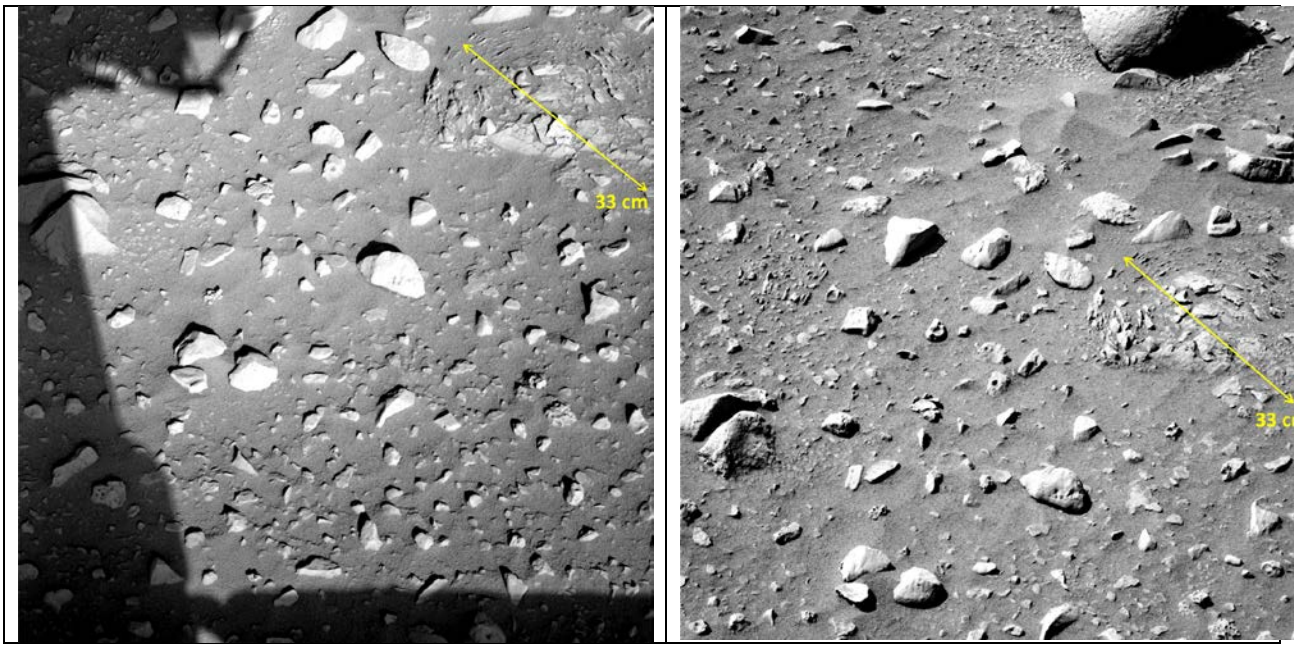

Fig. S6. Pancam images from the Spirit rover in Gusev crater, sols 103 and 105, showing a spherical exfoliation feature. The exposed portion is 33 cm in diameter.

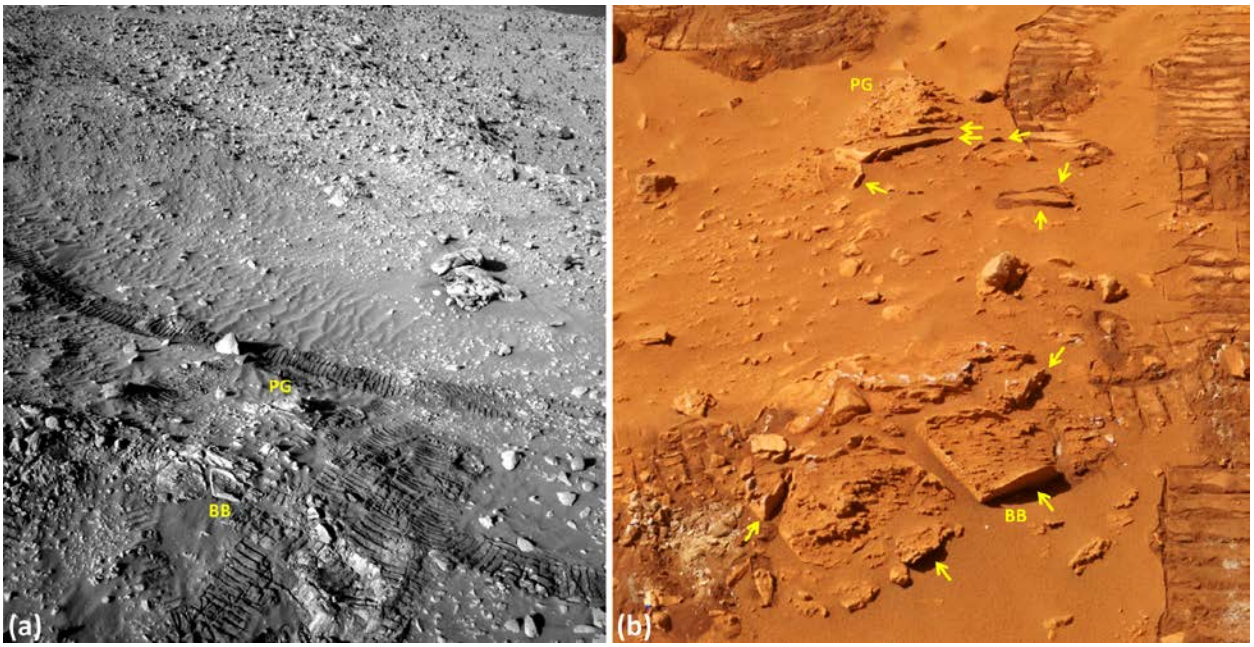

Fig. S7. Case hardening observed at Hanks Hollow, Columbia Hills, Gusev crater. (a) Navcam context image (sol 178) of targets Pot of Gold (PG) & Breadbox (BB). (b) High-resolution image (Pancam, sol 166) of PG & BB. Yellow arrows mark resistant shells that incase soft, easily eroded interiors. Scale is provided by wheel tracks (MER wheels are 16 cm wide).

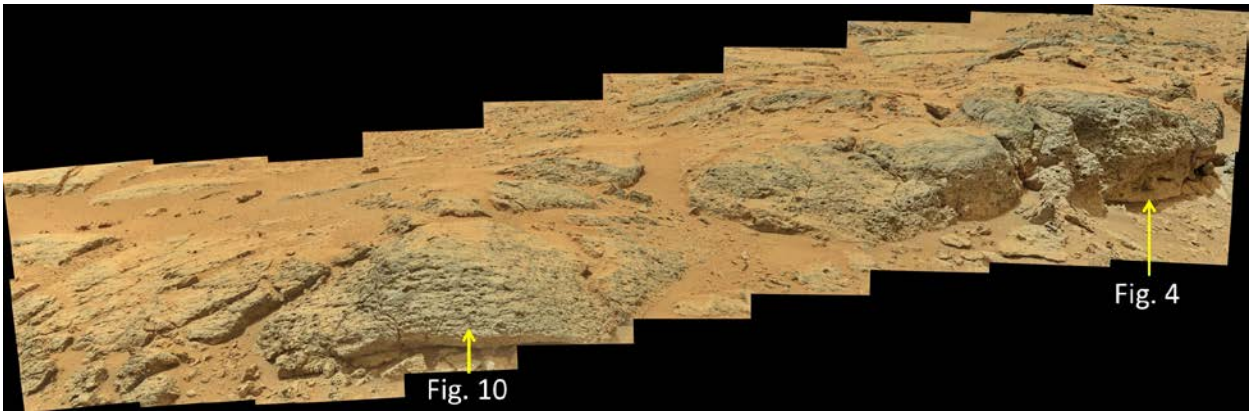

Fig. S8. Overview of the Point Lake outcrop showing the relative locations of features in Figs. 4 and 10.

Supporting Online Material:

MSL images used in this work:

Fig. 3. Tochatwi:
(a) Navcam, sol 121, NLA_408244754EDR_F0050926NCAM00216M1
(b-d) sol 122, 0122MR0007650000200768E01

Fig. 4. Point Lake: Mastcam images
Sols 302 & 305,
0302MR0012570100203802E01,
0305MR0012620110203874E01,
0305MR0012620080203871E01

Fig. 5. Twin Cairns Island: Mastcam images
Sol 343,
0343MR0013880020301096E01
0343MR0013880040301098E01

Fig. 6. Winnipesaukee,
Sol 654, Mastcam 0654MR0027730000401977E01,
RMIs: CR0_455554069PRC_F0340416CCAM01653,
CR0_455555129PRC_F0340416CCAM01653

Fig. 9. Snake,
Both the main image and the inset are from an MCAM 360° panorama acquired on sol 173 (sequence: mcam00926).
The image shown in the Figure is mainly: 0173MR0009260660201874E01

Fig. 10. Point Lake, MAHLI image sol 303, 0303MH0002890000103772R00

Fig. S1. Tochatwi and nearby features
(a) Tochatwi, sol 121, NLA_408244754EDR_F0050926NCAM00216M1
(Both insets are from the same image frame, i.e. 0122MR0007650000200768E01)
(b) Sol 123, NLA_408420207EDR_F0051070NCAM00218M1
(c) Sol 123, NLA_408420313EDR_F0051070NCAM00218M1

Fig. S2. Shaler pitted layer, sol 121, Mastcam 0121MR0007560110200724E01

Fig. S3. Sol 306 hollow spheroid near Shaler, Mastcam 0306MR0012670140203944E01

Fig. S4. Pitted object near Shaler, sol 308, Mastcam 0308MR0012730520204018E01

Fig. S5. Kimberley, sol 597, Mastcam 0597ML0025180020301189E01

Fig. S6: Images acquired by Pancam/MER (Spirit) through filter L7 (430 nm):
(Left) sol 103, 2P135521029EFF3000P2450L7M1,
(Right) sol 105, 2P135681301EFF3000P2387L7M1
Both images show the same feature, but acquired at different sols and from different vantage points.

Fig. S7: Images acquired by MER-A/Spirit:
(a) sol 178, Navcam, 2N142181330EFF69AKP0670R0M1sol 166
(b) Pancam sequence P2530, color composite

Fig. S8, mosaic indicating relative positions of Figs. 4 and 10 in the Point Lake outcrop: Sol 302, mcam01257 (mosaic of 20 images):
0302MR0012570000203792E01
0302MR0012570010203793E01
0302MR0012570020203794E01
0302MR0012570030203795E01
0302MR0012570040203796E01
0302MR0012570050203797E01
0302MR0012570060203798E01
0302MR0012570070203799E01
0302MR0012570080203800E01
0302MR0012570090203801E01
0302MR0012570100203802E01
0302MR0012570110203803E01
0302MR0012570120203804E01
0302MR0012570130203805E01
0302MR0012570140203806E01
0302MR0012570150203807E01
0302MR0012570160203808E01
0302MR0012570170203809E01
0302MR0012570180203810E01
0302MR0012570190203811E01